EFG RIBBON GROWTH

K. V. Ravi

Mobil Tyco Solar Energy Corporation
Waltham, Massachusetts 02154

The review will cover two projects entitled "Continuous Silicon Solar Cells" (Harvard-Tyco) and "Scale-Up of Program on Continuous Silicon Solar Cells."

Past activities in the theoretical aspects of EFG ribbon growth have dealt with capillary effects, die effects, thermal effects and crystal shape effects. This program was concluded in March and the final report is near completion. Effort since the last review meeting has been devoted to the examination of the shape of the meniscus at the ribbon edges. It has been determined that the height of the meniscus at the ribbon edges was underestimated in the earlier theory. Present theoretical findings along with analogue experiments indicate that the side meniscus lifts the edge meniscus effectively increasing the meniscus height at the edges. This finding has important consequences in the stable growth of high quality ribbons. Other factors considered include the effects of crystal orientation on ribbon shape or morphology.

The experimental aspects of growth have dealt with continuous ribbon growth and factors contributing to ribbon quality. Continuous ribbons of up to 80 ft (1 in. wide, 8 to 10 mils thick) in length have been grown. With the use of top or die heaters in resistance heated crystal growth systems, the control of vertical temperature gradients as well as the height of the meniscus above the die is possible. By employing a high meniscus mode of operation of the system a few crystals of very high quality with respect to defect densities (dislocations, twins and SiC particles) have been grown. The crystals also maintain a constant orientation over long lengths.

The quality aspects of ribbon crystals have been under continuous investigation with new insights into the characteristics of linear boundaries and SiC particles being developed.

A summary of the states of EFG ribbons was presented in the IEEE 11th Annual Photovoltaic Specialists Conference.

TITLE PAGE

I

TITLE:	CONTINUOUS SILICON SOLAR CELLS
ORGANIZATIONS:	HARVARD UNIVERSITY/TYCO LABORATORIES, INC.
PERIOD:	MARCH 1973 - MARCH 1975
AMOUNT:	$300,700 TOTAL HARVARD $111,000
	TYCO 189,700

PRINCIPAL
INVESTIGATORS: PROFESSOR BRUCE CHALMERS - HARVARD
DR. A. I. MLAVSKY   - TYCO

II

TITLE:	SCALE-UP OF PROGRAM ON CONTINUOUS SILICON SOLAR CELLS
ORGANIZATION:	MOBIL TYCO SOLAR ENERGY CORPORATION
PERIOD:	MAY 1974 - JULY 1975
AMOUNT:	$321,000

PRINCIPAL
INVESTIGATOR: DR. A. I. MLAVSKY

THEORETICAL CONSIDERATIONS

1. CAPILLARY EFFECTS

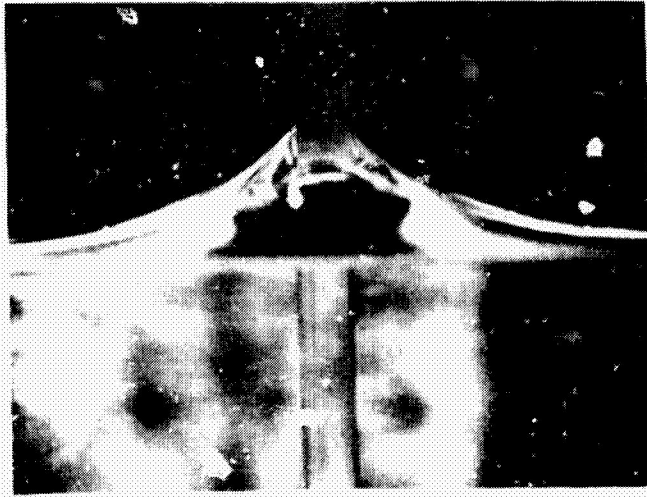2. DIE EFFECTS

3. THERMAL EFFECTS

4. CRYSTAL SHAPE EFFECTS
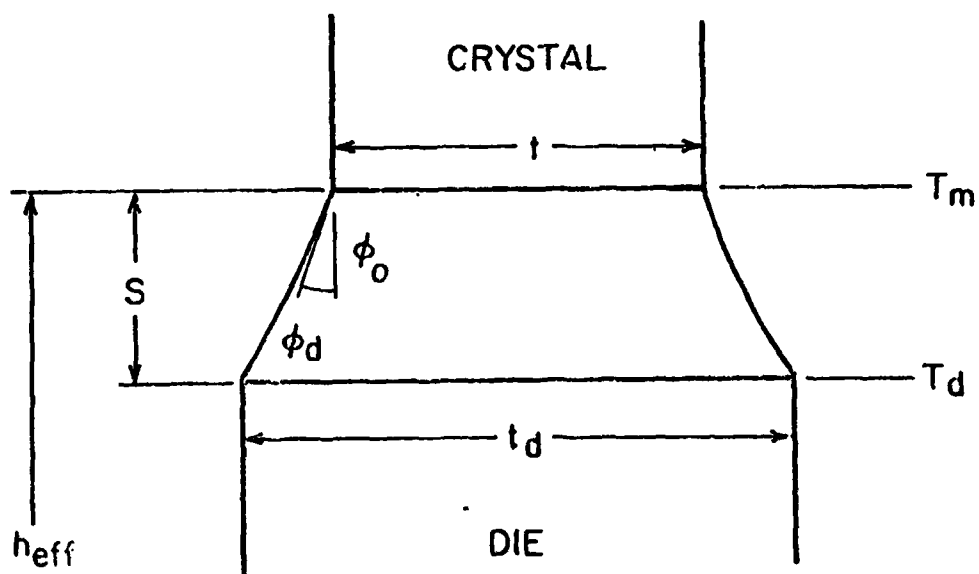
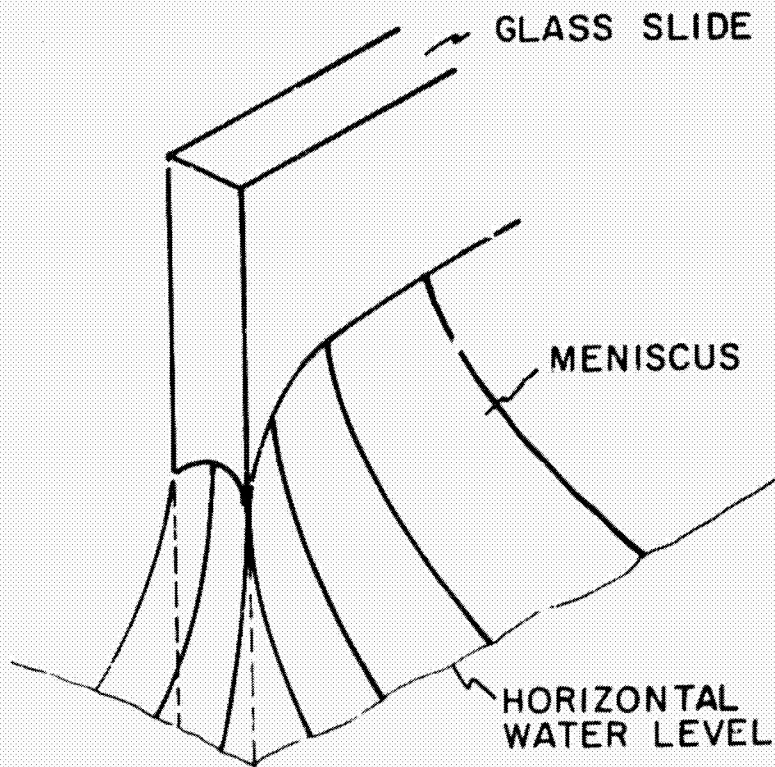REQUIREMENT FOR CONSTANT CROSS-SECTION GROWTH OF SILICON:

$\phi_o = 11° \pm 1°$ FOR {111} ORIENTATION

$\phi_o < 11°$ FOR OTHER ORIENTATIONS

THE ANISOTROPY OF ϕ_o AFFECTS THE RIBBON MORPHOLOGY.

(a)

GLASS SLIDE

MENISCUS

HORIZONTAL
WATER LEVEL

(b)

Axis labels for main plot:
- y-axis: $G / f(\beta)$, °K/cm, with values 0, 400, 800, 1200, 1600
- x-axis: $V / f(\beta)$, cm/sec, with values 0, .08, .16, .24

Line labels: t, cm — .05, .04, .03, .02, .01

Inset plot:
- y-axis: $f(\beta)$, with values 0, .2, .4, .6, .8, 1.0
- x-axis: T_o, °K, with values 400, 800, 1200, 1600
- $\beta = T_m / T_o$
- T_m
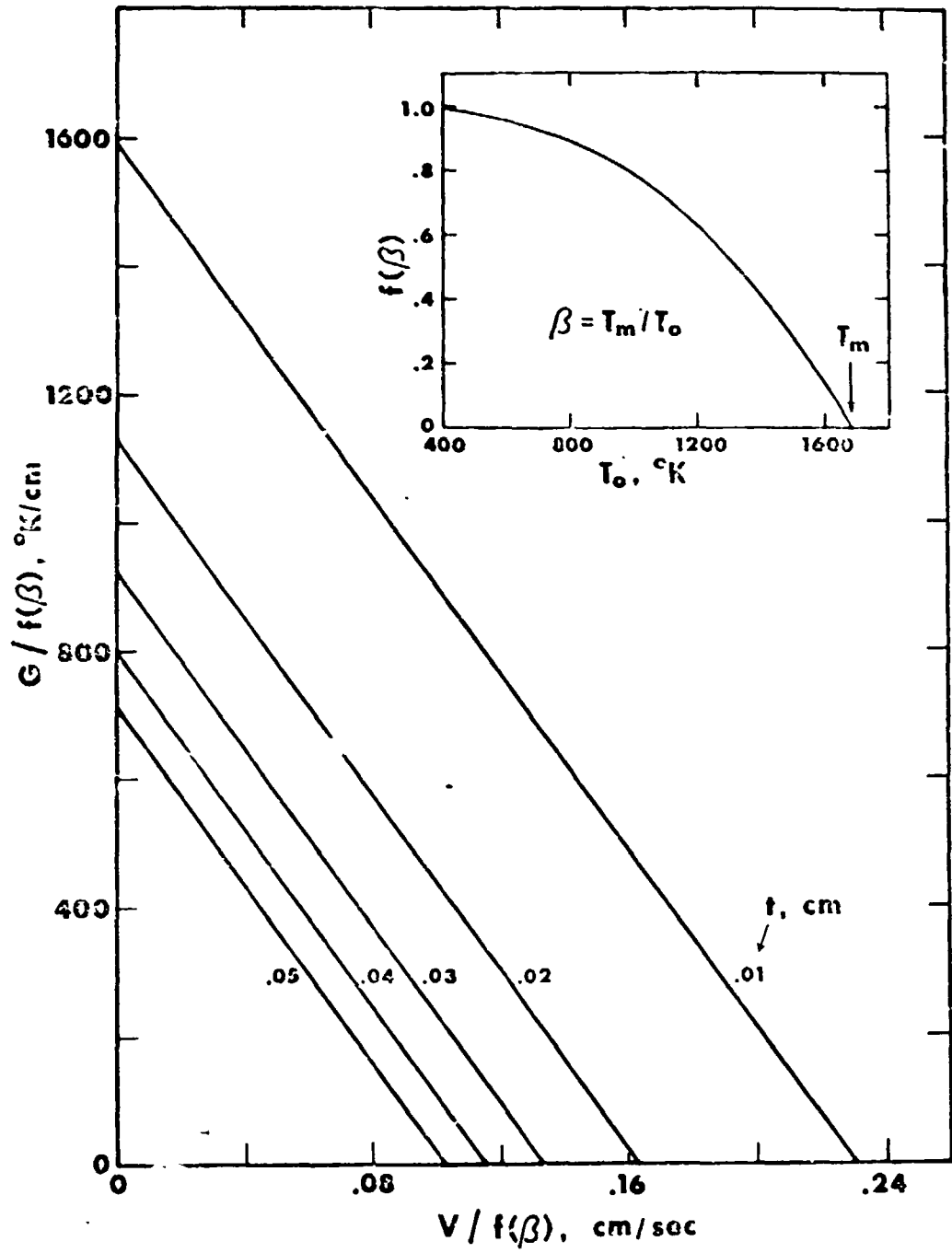
EQUIPMENT AND PROCESS DEVELOPMENT

1. RF HEATED SYSTEM -- PROBLEMS RELATING TO CONTINUOUS GROWTH.

2. RESISTANCE HEATED SYSTEMS -- PROBLEMS RELATING TO CONTINUOUS GROWTH AND CRYSTALLINITY CONSIDERATIONS.

PROBLEMS ADDRESSED IN CONTINUOUS RIBBON GROWTH

1. SCALE UP OF CRUCIBLE AND ASSOCIATED COMPONENTS.

2. DIE DESIGN FOR MENISCUS CONTROL AND MENISCUS DIMENSIONS.

3. RIBBON GUIDANCE AND COLLECTION OR SPOOLING APPARATUS.

CONTINUOUS RIBBON GROWTH - CURRENT STATUS

| MAXIMUM LENGTH	WIDTH	THICKNESS (AVERAGE)	GROWTH RATE (AVERAGE)	COMMENTS
80 FT	1 IN.	~8-10 MILS	~1 IN./MIN	RUN TERMINATED DUE TO DEPLETION OF MELT.
60 FT	1 IN.	~3-10 MILS	~1 IN./MIN	RUN TERMINATED.
40 FT	1 IN.	~8-10 MILS	~1 IN./MIN	RUN TERMINATED

PROBLEMS ADDRESSED IN RIBBON QUALITY

1. CONTROL OF VERTICAL TEMPERATURE GRADIENTS.

2. MENISCUS CONTROL CONSIDERATIONS.

3. HIGH MENISCUS MODE (HMM) OF OPERATION.
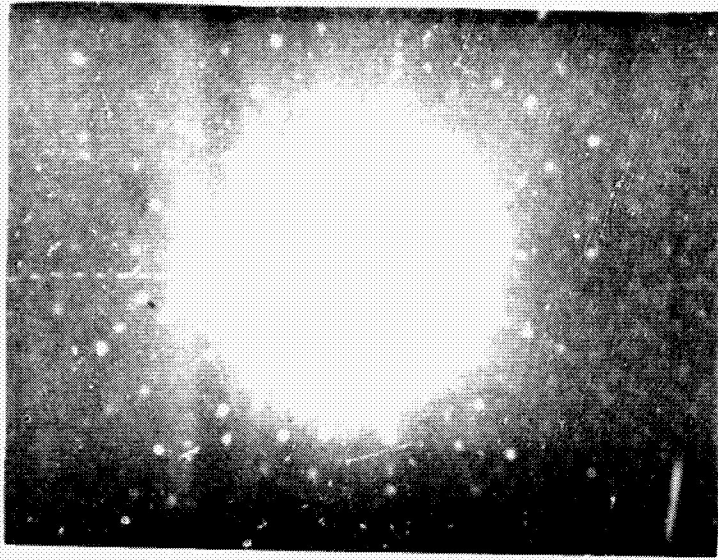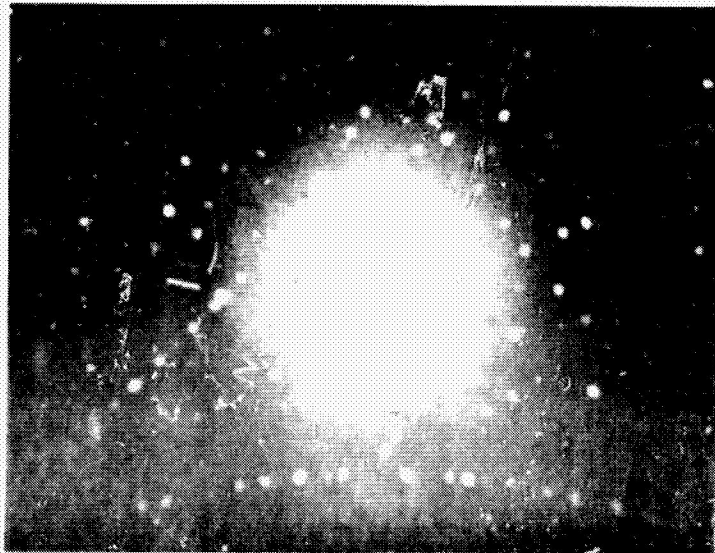
SEED - GROWTH PLANE (i11)
GROWTH DIRECTION [$\bar{2}11$]
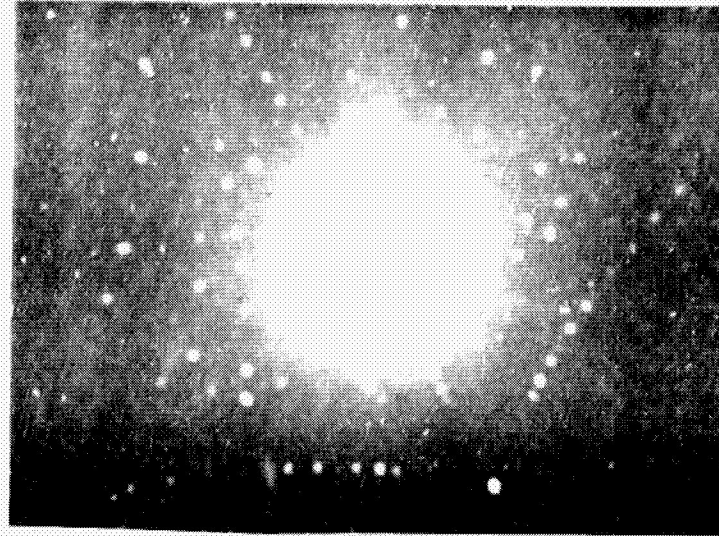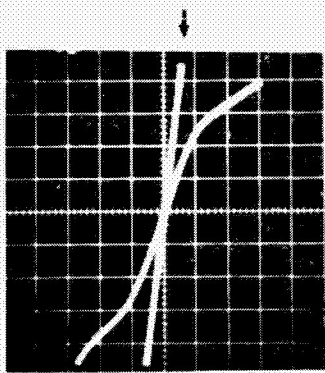
5 CM FROM SEED - 35° FROM (111)

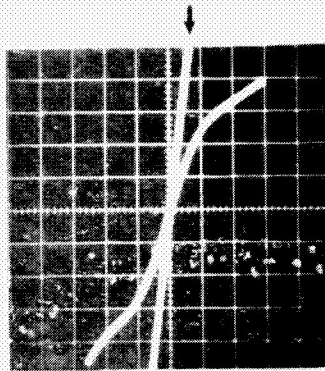14.5 CM FROM SEED - 16° FROM (111)

45 CM FROM SEED - 16° FROM (111)

1·5 Ω - cm FZ →

1-3 1-2 2-4

1mm

1 2

4 3

1-4 2-3

3-4

1·5 Ω - cm FZ →   SAMPLE : 14-55-3-7

114

2-4

1-2

1-3

2-3

1mm

2   1

3   4

1-4

3-4
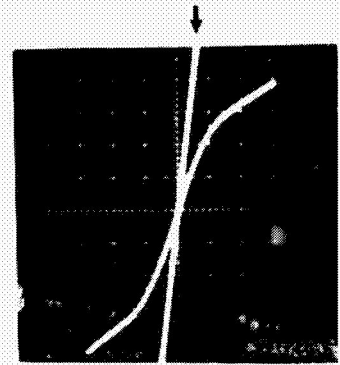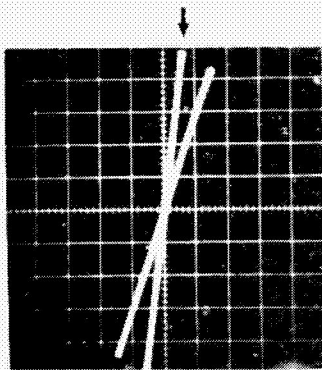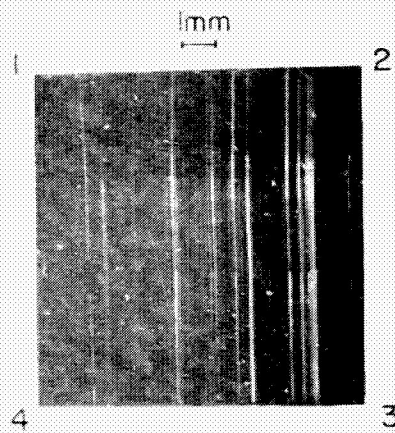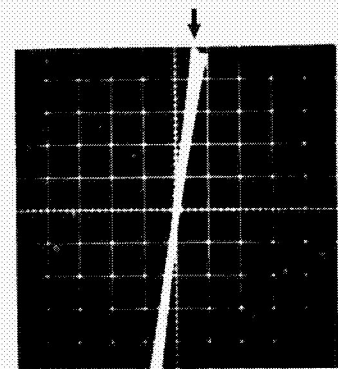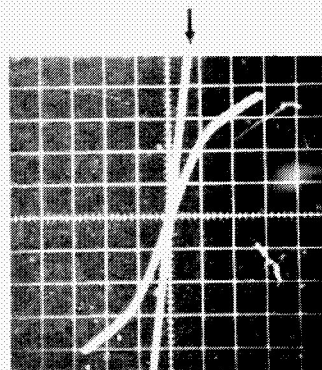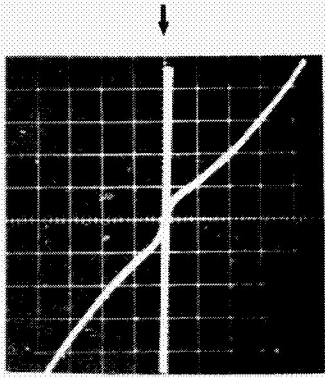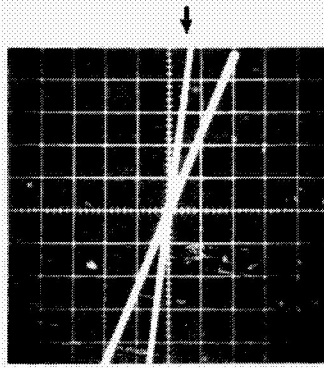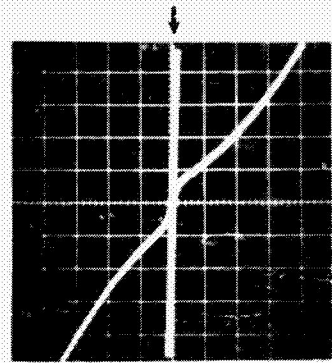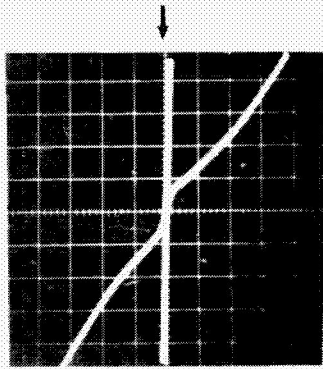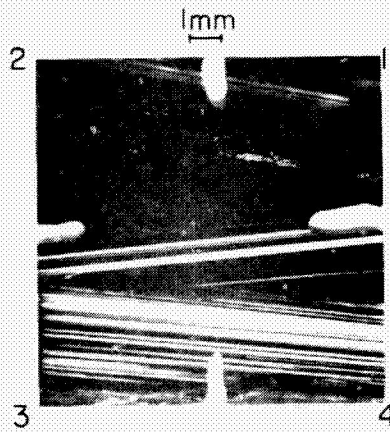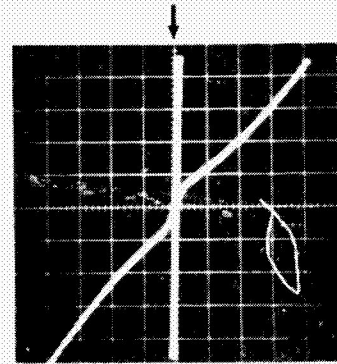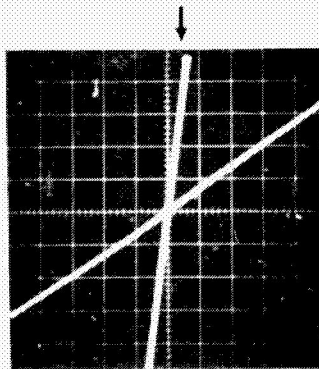
1.5 Ω-cm FZ →   SAMPLE 14-38-3-4

1-3

1-2

1mm

2-4

1-4

4

2

3

2-3

3-4
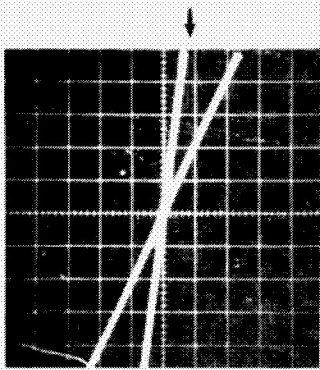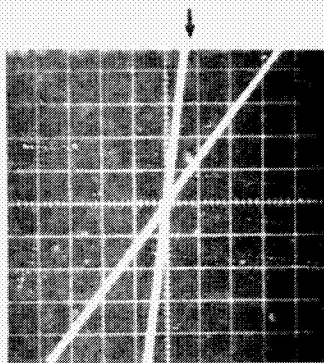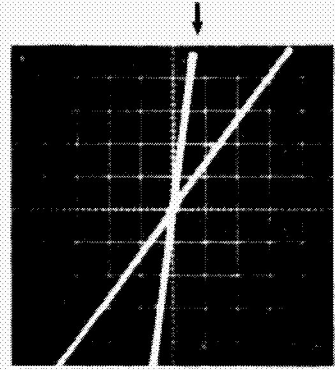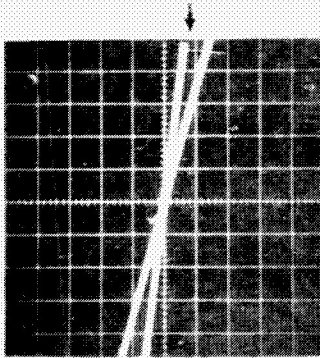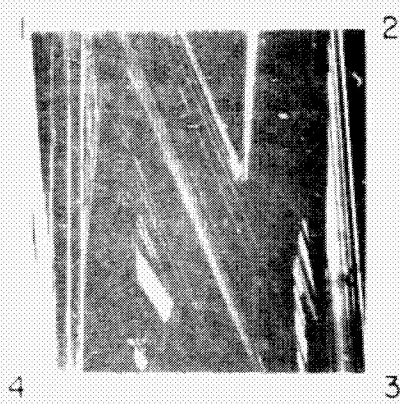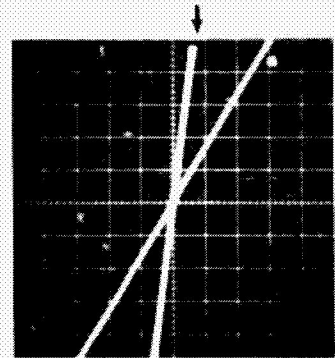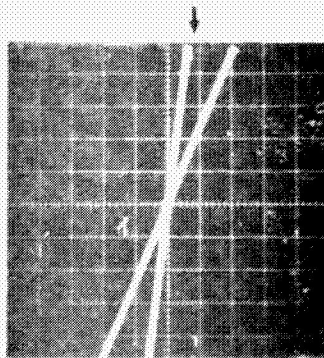
15 Ω-cm FZ →

SAMPLE 14-39-4-5

50 μm
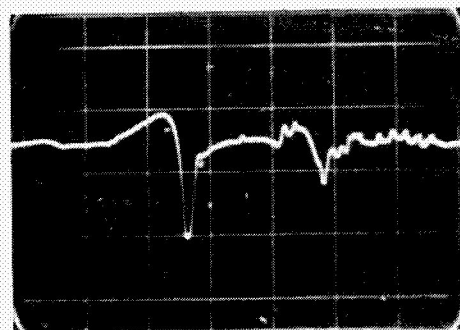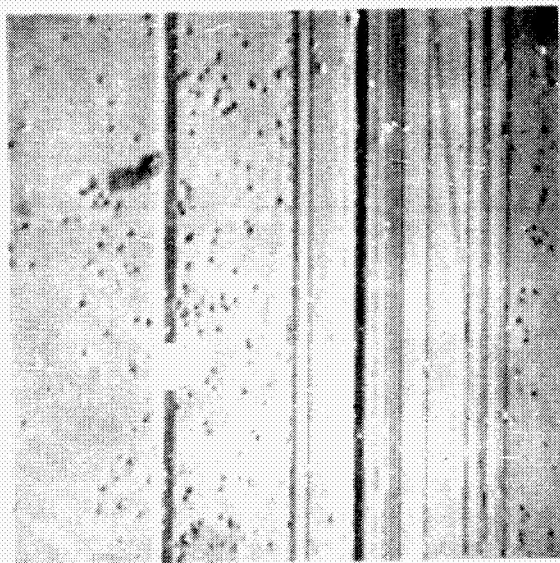
SCAN DIRECTION ⟶

SCAN DIRECTION ↓

SILICON RIBBON N-P SOLAR CELL

$V_{SPV} = 500\ \mu V$

$V_{SPV} = 250\ \mu V$

$I_0\ (I-R)$ (ARBITRARY UNITS) →

$L_D = 77\mu$

(ABSORPTION COEF) $^{-1}$ →

118

RELATIONSHIP OF I_{SC} VS. L_D IN
RIBBON SOLAR CELLS
N-P JUNCTION

L_D DIFFUSION LENGTH (μ) ⟶

I_{SC} (MA/CM^2) ⟶
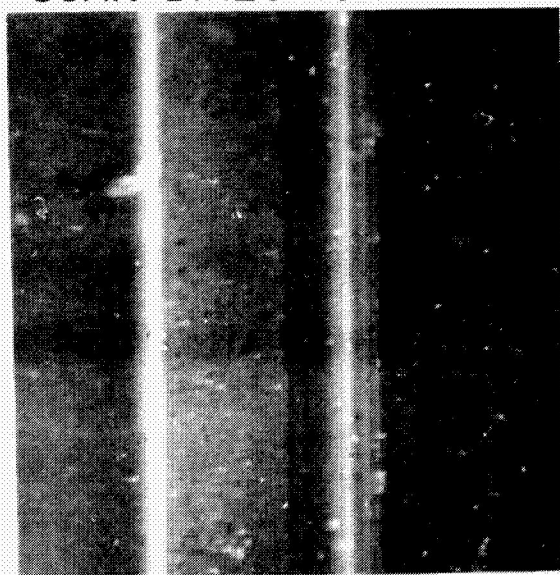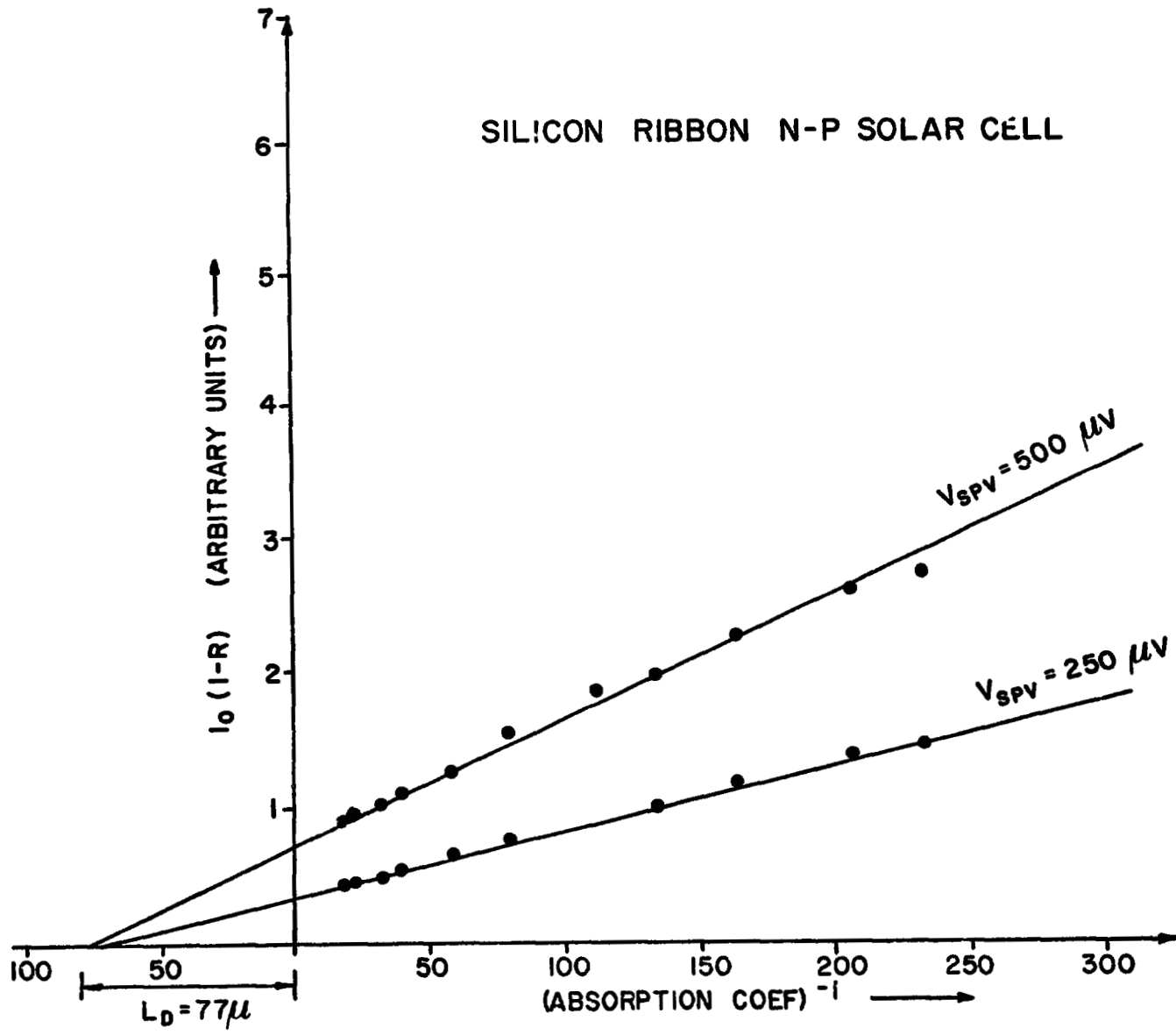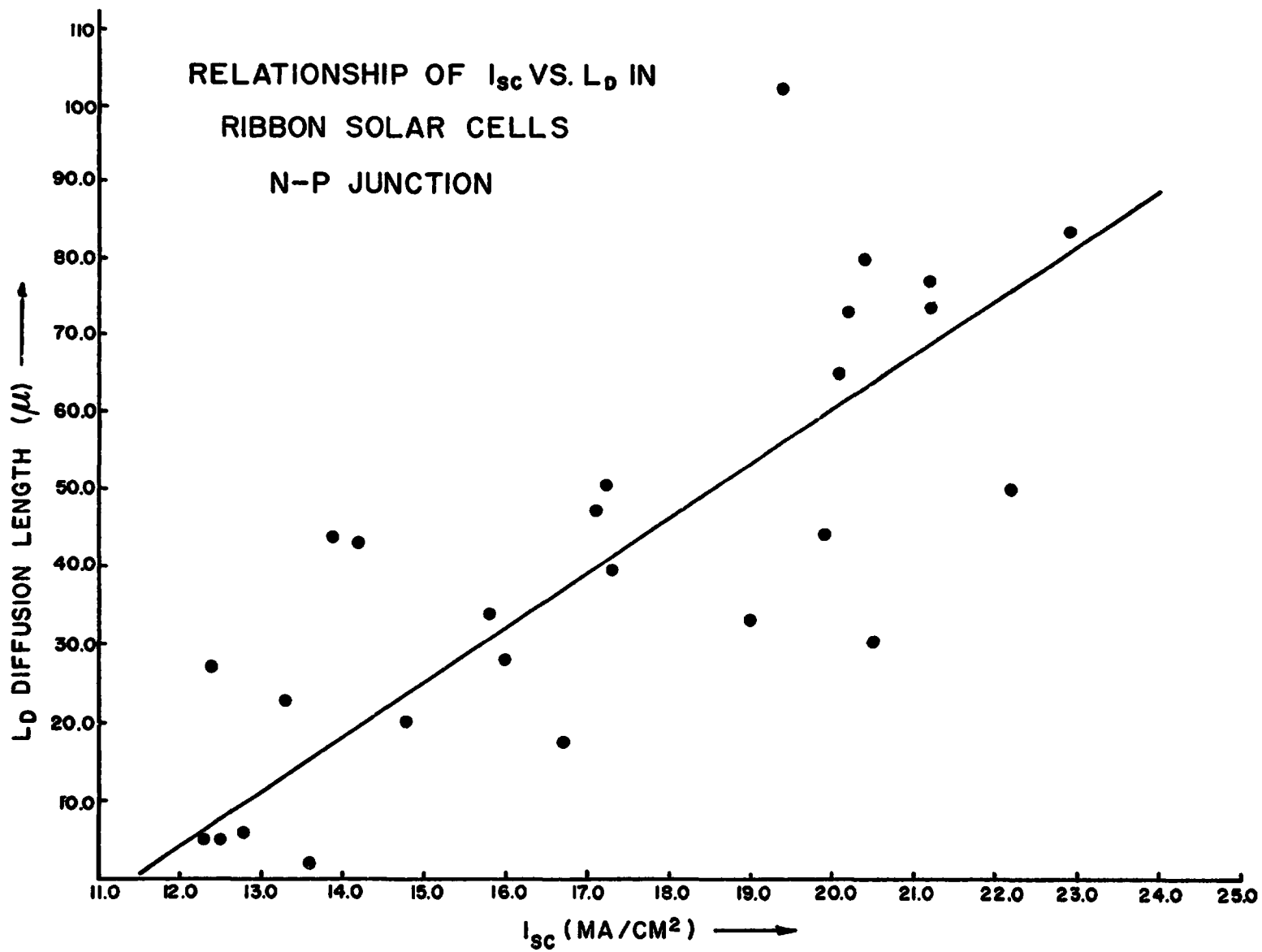
SUMMARY OF KEY RESULTS

1. THEORETICAL UNDERSTANDING OF MENISCUS SHAPE AND STABILITY AT RIBBON EDGES.

2. THEORETICAL RELATIONSHIPS BETWEEN CRYSTAL ORIENTATION AND RIBBON DIMENSIONS HAVE BEEN DETERMINED.

3. FACTORS RELATING TO THERMAL EFFECTS AND CRYSTAL SHAPE CONTROL HAVE BEEN ANALYZED.

4. CONTINUOUS RIBBON GROWTH HAS BEEN ACHIEVED WITH THE MAXIMUM LENGTH TO DATE BEING 80 FT (1 IN. WIDE, 8-10 MILS THICK).

5. THE STRUCTURAL CHARACTERISTICS OF RIBBONS AND STRUCTURE – PROPERTY RELATIONSHIPS HAVE BEEN STUDIED.

6. A FEW HIGH QUALITY RIBBONS WHICH PROPAGATE AND MAINTAIN SEED ORIENTATIONS HAVE BEEN GROWN. THIS GROWTH HAS BEEN ACHIEVED WITH THE HIGH MENISCUS MODE OF OPERATION OF THE SYSTEM.

STATUS SUMMARY

A. BASIS ESTABLISHED FOR EXPERIMENTAL DEVELOPMENT OF
    FAST, WIDE RIBBON.

B. CONDITIONS ESTABLISHED FOR CONTINUOUS UNATTENDED GROWTH.

C. EFFECT OF GROWTH PARAMETERS ON QUALITY UNDERSTOOD TO
    PERMIT SYSTEMATIC QUALITY IMPROVEMENT

$$- A + B + C -$$

LOW COST HIGH QUALITY SHEET PRODUCTION

EFG SILICON RIBBON SOLAR CELLS

K. V. Ravi, H. B. Serreze, H. E. Bates, A. D. Morrison
D. N. Jewett and J. C. T. Ho

Mobil Tyco Solar Energy Corporation
W? .am, Massachusetts 02154

Presented at the

11th

**PHOTOVOLTAIC
SPECIALISTS
CONFERENCE**

PHOENIX, ARIZONA

MAY 6-8, 1975

EFG SILICON RIBBON SOLAR CELLS

K. V. Ravi, H. B. Serreze, H. . . Bates, A. D. Morrison
D. N. Jewett and J. C. T. Ho

Mobil Tyco Solar Energy Corporation
Waltham, Massachusetts 02154

SUMMARY

The growth and characteristics of edge-defined, film-fed grown (EFG) silicon ribbons are discussed. Factors involved in the growth of continuous lengths of 1 in. wide ribbons are examined. The structural and electrical characteristics of the ribbons have been studied and the results are presented. Solar cells have been fabricated using the ribbon crystals and typical AM0 efficiencies of 6 to 10% have been realized.

INTRODUCTION

Among the principal factors that affect economically and technically the attainment of large scale silicon photovoltaic systems is crystal growth. The cost factors associated with the conventional Czochralski growth technique are such that alternative procedures for obtaining single crystal silicon in ribbon form by direct solidification from the melt are desirable. One such technique is the edge-defined, film-fed growth (EFG) process whose features have been discussed elsewhere (1, 2). Initial results of ribbon growth experiments relating to silicon were reported in previous meetings of this conference (3, 4) and elsewhere (4a). It is the intent here to present an update of this technology. A discussion of the growth aspects of silicon ribbon is followed by a description of the structural characteristics of the state-of-the-art ribbon. Structure property relationships have been studied with specific

123

emphasis on the effects of linear defect boundaries on photo-generated signals in the material. Data on ribbon solar cells is presented in the concluding section of this paper.

RIBBON GROWTH

The most prominent characteristic of the EFG technique is the ability to grow ribbons of a given dimension with good shape control. In order to attain this dimensional control, a die is inserted between the bulk of the melt and the growing interface. This produces several advantages, but also certain engineering constraints which must be considered in the growth of silicon ribbons by EFG.

Briefly, the advantages of the EFG process are: the isolation of the growth interface from the bulk of the melt; the production of an interface which stays at a constant location relative to the isotherms in the system - instead of fluctuating up and down with the melt - the development of a fluid flow system which ensures that the composition of the ribbon will be that of the melt feeding the ribbon; and, of course, direct shaping of the crystal. The basic requirement is the existence of a die material which is wet by, but which does not significantly react with molten silicon.

The die material currently being used is graphite. Graphite presents a number of problems which have to be overcome in its use as a die for EFG. The most apparent problem is the formation of silicon carbide in the form of a layer and in particulate form within and on top of the die during ribbon growth. The particles, about 0.05 to 0.1 mm in the largest dimension, create a rough surface on the die. They often protrude from the bottom of the meniscus, appearing cold and black in contrast to the meniscus of molten silicon. These cold precipitates cause projections of the growth interface towards the cold region. These projections cause a rough solid-liquid interface thereby leading to instability and, possibly, structural defects.

Although graphite reacts with molten silicon, the reaction rates have been observed to be slow enough for the successful development of ribbon growth technology. Up to 65 feet of ribbon has been grown from a single die. Examination of the dies following the sustained growth of long lengths of ribbon has not revealed the presence of significantly more SiC on top of the die as compared to carbide formation on dies through which small lengths of ribbon (< 10 ft) have been grown. Typical examples of dies from which short and long ribbons have been grown are shown in Fig. 1. Further, die erosion or distortion effects were not observed in any of the dies used for long growth runs.

The die, which provides the advantages of shaping, isolation from the melt, etc. also imposes certain requirements in terms of design of the die and of the thermal environment surrounding the die. In addition, certain operating or process constraints exist which have to be considered in order to achieve successful growth. For example, the amount of melt which is in proximity to the growing ribbon is quite small in comparison to Czochralski growth. Therefore, loss of very small amounts of heat can provide enough of a temperature decrease to cause solidification of the ribbon at the die top.

Silicon has approximately twice the thermal conductivity of graphite. As a result, more heat flux per cross sectional area travels up the column of liquid silicon than up the graphite die. In addition, the outside and top edges of the die tend to be cold with respect to the molten silicon, since in typical rf heated systems, the outer sloping face of the die is free to radiate heat away, and the only source of heat to that portion of the die is the die holder or lower structures. In this case the interface will tend to curve downward towards the die edges; if the temperature of the liquid near the die top approaches the melting point, there will be a tendency for the interface to advance towards the die edges.

There are other areas where a detailed consideration of the thermal environment at the top of the die is crucial. For instance in spreading a small seed into a full width ribbon there are several different thermal stages which are observed. Before seeding takes place, the temperature along the top of the die is nearly uniform and is just above the melting point. Upon seeding there is additional heat loss up the seed by means of conduction which tends to decrease the temperature at the top of the die and cause the silicon to freeze. Heat is added at this time in order to remelt the silicon, or cally the melt temperature is raised before seeding to allow for this heat lr the seed has been melted and the meniscus has been established, growth may in. However, at this point the silicon at either side of the seed is much hotter than the silicon directly under the seed. Therefore, the ribbon will tend to taper instead of spreading. In order to overcome this tapering, growth speed is increased rapidly until the heat of solidification at the narrow seed is generated rapidly enough to compensate for extra heat lost up the seed. At this point the silicon under the growing seed may be hotter than the silicon on either side of the seed, and the ribbon will then spread in response to the temperature gradient.

One difficulty with this approach is that the growth rate mus ͼ raised very rapidly to a high level and this may entail dropping the heat input to the top of the die to such an extent that the rest of the silicon freezes and the growth is aborted. Full width seeding with a growth system which is essentially isothermal along the die top has been developed to avoid this situation. The edges of the die and ribbon radiate enough extra heat away to allow the ribbon to stay at full width.

In developing this technology, three meniscus shapes (Fig. 2) have been used as simple guides to the thermal environment during ribbon growth. The first shape, (Fig. 2A) concave with respect to the ribbon (meniscus closer to the die at the center), is attained when the ends of the ribbon are hot with respect to the center of the die. Growing with this meniscus shape causes the ribbon to taper. Attempts to spread the ribbon by decreasing the temperature lead to freezing of the ribbon to the center of the die.

The opposite thermal condition (Fig. 2B), the ends of the ribbon cold with respect to the center, leads to a meniscus convex with respect to the ribbon (meniscus closer to the die at the ends). In this case the ribbon will spread rapidly, but it is difficult to prevent the edges of the ribbon from freezing to the die.

Finally, a meniscus curved up on one end and down on the other results from one end being hotter than the other. A ribbon grown in this environment tends to taper on one side and spread on the opposite (Fig. 2C). This phenomenon is also caused by having the die, susceptor, heat shields, or other components slightly out of balance. Tightening of component specifications and special care in assembly of the growth set up are the major ways to avoid this problem. The vertical gradient variations are also crucially important. These gradients determine allowable growth speeds, sensitivity of meniscus height to changing growth speeds, etc.

Silicon ribbons have been grown from three different types of furnaces and with three types of pulling mechanisms. The initial experimental work was done with high frequency induction systems. These are characterized by simple growth set up design, good visibility and rapid power adjustment capability. The disadvantages include higher power consumption, rf interference in control devices, and the presence of a single power zone. The motor generator induction furnace has the advantages of the rf system but uses less power and produces less electronic interference. It still is characterized by one hot zone. Fig. 3 shows a typical example of an rf heated growth station.

126

The resistance furnaces which have been more recently developed have independent top heating zones which permit the attainment of continuously variable thermal gradients within the die. In addition, the combination of reliability, low power consumption (a factor of 3 less than rf heating), low electronic interference, and design flexibility make this approach more desirable. Its drawbacks are associated with the more complicated, larger system enclosures and the added requirements imposed on heating element design. Fig. 4 shows an example of a resistance heated system.

Two types of vertical pulling mechanism have been used. The hydraulic piston system first used provides a very smooth stroke, but it is quite bulky, not easily controllable and difficult to monitor. The second type uses a motor driven ball screw assembly which, with suitable mechanical damping, provides easily controlled and monitored pulling. Finally, two different continuous belt puller designs have been used to grow continuous ribbon. The advantages of electric control and monitoring are still present, and of course there is an unlimited pull stroke. The major problems are providing adequate mechanical guide . the ribbon, avoiding ribbon "wander" within the belts of the pullers, and in the ing of seed holders which can move through the belts with a minimum of disturbance in the transition from seed holder to ribbon. All of these systems have been used to successfully grow 1 inch wide ribbons. As mentioned above, ribbons of lengths up to 65 feet have been grown employing continuous belt pullers. The ribbons have been sufficiently strain free to permit reeling on to ~ 3 ft diameter reels. Fig. 5 shows the reeling mechanism on a growth station.

RIBBON CHARACTERISTICS

The two most significant ribbon characteristics in addition to dimensional control are the chemical purity and crystallographic structure.

Chemical Purity

Because of the intimate contact between the liquid and the die during the growth process it is necessary not only that the die material itself not introduce significant numbers of electrically active impurities, but also that impurities in (and on) the die be minimized. Carbon is electrically inactive in silicon; however, the total impurity content of typical high purity commercial graphites can be of the order of 100 to 600 ppm. Transition metals are generally present as major fractions

of the total, as are aluminum and silicon. Fabrication and handling of graphite dies can also, of course, introduce a broad spectrum of impurities. Since nothing is known about the kinetics of impurity transfer from the bulk of the die to the melt, it is safest to assume that all impurity atoms present in the die will be immediately introduced into the melt, and thus to strive to lower the impurity levels in the graphite as far as possible. As an example, it is found that the typical graphite die material being used (DFP-2 grade having been subjected to a high temperature purification treatment by the manufacturer) contains approximately 5 ppm of iron. This translates into approximately 6×10^{16} atoms of iron in a 2.5 cm wide by 3.05 cm long, ~0.5 cm thick graphite die.

A typical melt used with this size die contains about 10 cm^3 of silicon. Complete transfer of the Fe to the melt would then produce a level of 4×10^{15} atoms/cm^3 of Fe in the silicon. If in fact only 10% of the total finds its way into the melt, the resulting 4×10^{14} atoms/cm^3 of Fe is still a fairly high concentration for a deep level impurity. Given these considerations, the course of effort followed to achieve suitable low impurity levels in graphite dies is discussed below.

Vacuum Firing

The first approach to cleaning graphite dies was vacuum outgassing. This process evolved from a fairly mild 1500°C, 10^{-2} torr treatment which probably only removed the more volatile contaminants introduced during fabrication, giving typical ribbon resistivities of 0.5 Ω-cm, to a 1900°C, 10^{-5} torr, one hour treatment, which, when applied to dies made from DFP-2 (i.e., pre-purified) graphite allowed fairly consistent growth of ribbon of 1 to 2 Ω-cm, p-type resistivity. Solar cells produced from these ribbons typically performed at about 1/2 to 2/3 the level of control cells made from commercial Czochralski silicon. Spectral response data, showing reduced red-response for the EFG-ribbon cells relative to the Czochralski cells, were taken to indicate the presence of lifetime killing impurities which presumably were not being removed by the vacuum-firing treatment.

Hydrogen Chloride Firing

The use of high temperature treatments in chlorine or fluorine-containing atmospheres for the production of nuclear-grade and spectrographic graphites is fairly well-known (5). The treatment works by diffusion of impurity atoms from within the bulk of the graphite grains to their surfaces, there to react with the halogen atoms forming volatile halides which are carried away in the gas phase.

Consequently, a procedure for the post fabrication purification of the dies has been established involving the heating of the dies at temperatures of ~1300°C in an atmosphere of argon and anhydrous HCl with a 5% HCl content by volume. The purification times are typically 5 hours. As a result of this process significant improvements in purity have been observed as evidenced by electrical measurements and solar cell data from ribbons grown from purified dies.

Crystallographic Structure

Typical ribbon crystals currently being grown by the EFG process are characterized by a large density of crystallographic defects. A detailed analysis of defect types and densities in many ribbons has been made and the following is a brief discussion of these characteristics. By far the most predominant defect types observed are twins and dislocations with occasional low angle grain boundaries. In addition, silicon carbide (SiC) particles are observed as inclusions distributed randomly across the length and the width of the ribbon. Typical characteristics of current ribbons can be described as follows.

Twins

Twin boundaries of varying densities and orientations are observed. Both growth twins and deformation twins are formed, typical examples of which are in Fig. 6. Deformation twins are sometimes characterized by the presence of dislocations in their vicinity and appear as fine narrow bands, whereas growth twins are typically wide and generally free of dislocations. At least three modes of twin nucleation appear to be operative in the crystals. (a) Twins have been observed to nucleate at SiC particles embedded in the ribbon; a typical example is shown in Fig. 7. (b) twin nucleation at the seed-crystal interface is a common occurrence with both deformation twins and growth twins forming at the interface; examples of this are shown in Fig. 8. (c) growth instabilities represented by local changes in ribbon dimensions have also been observed to generate twins as shown in Fig. 9.

Dislocations

Most of the dislocations observed appear to be deformation induced. This is evident from the observation that the dislocations are aligned along close packed planes to form slip bands. A typical case is shown in Fig.10. Dislocation-twin interactions are frequently observed with local dislocation pile-ups (Fig. 11). Dislocation generation around SiC particles is also observed.

129

SiC Particles

The inclusion of SiC particles in ribbon crystals can occur as a result of three possible mechanisms; (a) precipitation of dissolved carbon in the solid in the form of SiC subsequent to solidification. (b) precipitation of SiC at the solid-liquid interface as a result of carbon rejection from the solidifying crystal into the meniscus, and (c) the pick-up of SiC particles by the interface from the top of the die with subsequent incorporation into the solid.

Although a definitive determination of the relative importance of these processes has not yet been obtained, initial studies indicate that by far the most frequently occurring process is the pick-up of SiC particles by the solid-liquid interface from the die and the attendant inclusion of the particles in the ribbon. Typical particle densities are in 1-2 particles/cm^2 range.

The influence of seed orientation on the morphology of linear boundaries (twins and arrayed dislocations) is observed to be quite marked. For example, ribbons with a $(110) <1\bar{1}2>$ orientation are found to have predominantly linear boundaries parallel to the ribbon edges.

A number of avenues are available for obtaining ribbon quality improvements. One approach is discussed here which involves the control of the vertical temperature gradient within the die to minimize the dissolution and reprecipitation of carbon in the form of SiC. A reduction in the vertical temperature gradient is achieved by the use of an independent top or die heater in a resistance heated crystal growth apparatus (Fig. 4). By suitably controlling the temperature at the die top the temperature difference between the silicon in the crucible and the silicon at the top of the die (the meniscus) can be kept at the minimum. By this means short lengths of ribbon have been grown with significantly reduced defect densities as compared with ribbons grown under conditions of large vertical temperature gradients within the die.

Table I shows the average defect densities observed in the ribbon. It is apparent that densities of both linear boundaries (twins and slip bands) and dislocations are lower in crystals grown from resistance heated systems employing die heaters to appropriately control temperature gradients.

Table II lists the average electrical properties of ribbon crystals with data on typical Czochralski crystals of similar resistivity for comparison. A characteristic that is immediately apparent is the relatively large range in properties observed in the ribbon crystals. This fact in addition to the largely linear morphology

Table I. Average Defect Densities of EFG Silicon Ribbons
(20 in. after growth initiation)

	RF Furnace	Resistance Furnace
Parallel Boundaries/cm	7.5×10^2	3.9×10^2
Dislocations/cm^2	1.2×10^6	3×10^5

(Data represents average values from 20 specimens grown in an rf heated apparatus and 10 specimens from a resistance furnace).

Table II. Average Electrical Properties of EFG Silicon Ribbon: Boron Doped - 1.1 Ω-cm.

	Average	Range	Typical Czochralski Values
Resistivity:	1.8 Ω-cm	0.4 - 5.2	1.8
Mobility:	215 cm^2/V·sec	60 - 320	350
Photoconductivity Decay Time:	8 μsec	0.2 - 37	15
Absorption Coefficient at 1.8 μm:	16 cm^{-1}	0.1 - 65	0.05 - 0.5

(Based on 33 samples from 14 ribbons grown from one rf system).

of defects observed in the ribbon, indicates that a full understanding of local defect-property relationships is required to obtain a complete characterization of the crystals.

STRUCTURE PROPERTY RELATIONSHIPS

The conversion efficiencies of silicon solar cells are dependent, among other things, upon the presence or absence of non-radiative recombination centers and upon defect-impurity factors that reduce the minority carrier lifetime in the bulk of the crystal. The presence of large densities of crystallographic defects and transition metals in ribbon crystals undoubtedly adversely affects solar cell properties. In order to determine the specific effects of defects on electrical characteristics, a relatively detailed examination of structure-property relationships is needed. A variety of procedures has been adopted to evaluate the specific electrical effects of particular defects. Among the most dominant defects, as previously discussed, are linear boundaries represented by twin and slip bands. These linear boundaries have been observed to exhibit highly anisotropic properties. The local electrical characteristics of the ribbons were determined by measuring the local photovoltage and photocurrent generated by a laser beam incident on a ribbon solar cell. By scanning the laser beam across the width of the ribbon and recording the photogenerated signal, it was possible to evaluate both the distribution of properties across the width, as well as the effects of local linear defect boundaries. Fig. 12 shows three typical traces of the short circuit current response produced in a ribbon solar cell by a scanned laser beam at three different regions of a long ribbon. Two effects are notable in these plots. The current response at the edges of the ribbon is markedly reduced in comparison with the response at regions removed in comparison with the response at regions removed from the edges, and localized small scale variations in the signal are evident across the entire ribbon width. The localized reduction in photocurrent has been directly related to the presence of linear boundaries. The optical micrograph in Fig. 12 indicates a set of parallel boundaries which cause the particular reduction in short circuit current shown by the arrows on the plots. A one-to-one correlation between the presence of linear boundaries and a local reduction in photogenerated signals has been observed.

When the defect morphology is more complicated, as in the case of intersecting boundaries, the effects on electrical characteristics are further exacerbated. This is demonstrated in Fig. 13 where the short circuit current generated at a region containing multiple intersecting boundaries is much lower than that generated in regions either free of boundaries or containing non-intersecting parallel boundaries.

This distinction in the properties of intersecting and non-intersecting boundaries has also been observed in the breakdown characteristics of mesa diodes fabricated in ribbon crystals (6) as well as in solar cell properties (7).

An indication of the range of light generated current response in a ribbon as a result of the presence of linear boundaries can be obtained by comparing the theoretically expected spectral response of a solar cell for different minority carrier diffusion lengths in the base material with the experimentally determined short circuit response at the wavelength of the laser beam (He-Ne laser with a wavelength of 633 nm). Fig. 14 shows a plot of the theoretically determined spectral response for different values of diffusion length. (See Appendix for a discussion of the theoretical basis used to obtain the plots in Fig. 14). The range of values for the collection efficiency (Q) at 633 nm obtained from the laser measurements is superimposed over the theoretical plots. Q values were calculated from Eq. 1 in the Appendix by taking the peak of short circuit photocurrent response due to the laser beam excitation (λ = 633 nm. No (incident photon flux density) = 4.8×10^{17} photons/cm^2 sec) as the maximum and the valley response as the minimum in the range. It is observed that the peak response corresponding to defect-free regions indicates that the diffusion length for minority carriers is $\sim 30\ \mu$ whereas the diffusion length at the linear boundaries is $\sim 5\ \mu$. A reduction in the minority carrier diffusion length of a factor of six results at the defect boundaries. This range, of course, is for a specific ribbon and could vary as a function of the particular processes, such as die purification techniques employed during ribbon growth.

The change in the diffusion length at the boundaries indicates either a reduction in the mobility or lifetime. This can be the result of the direct effect of the defect boundaries as a consequence of the strain associated with the boundaries or as a result of the presence of dangling bonds associated with dislocations. However, a detailed analysis of the I-V characteristics of ribbons containing linear boundaries suggests that an association of impurities with the boundaries is a more likely reason for the unusual electrical behavior (8). A more precise indication of the localized conduction behavior of linear boundaries was obtained by a scanning electron microscope operated in the electron beam induced current (EBIC) mode (9). This technique permits the investigation of the electrical effects of localized defect-impurity complexes in semiconductors (10, 11). The current generated in a diffused n$^+$p junction (a solar cell) by a scanning electron beam is amplified and displayed on a CRT. By

operating the instrument in a single line scan mode the local interaction between the beam generated carriers and the linear defects can be observed. Fig. 15 shows a secondary electron image of a set of linear boundaries. The waveform shows the EBIC signal obtained when the beam is scanned across the linear boundaries by employing a single line scan. The instrument was operated at 30 kV with a beam current of 200 μA and spot size of ~ 1500 Å. When the beam crosses a linear boundary a local reduction in the EBIC signal is observed. The waveform represents the net flow of charge carriers at the space charge region of the p n junction in the region containing the linear boundaries. The abrupt change in the EBIC signal indicates that the boundaries function as local regions of low minority carrier lifetime in the ribbons. Further discussion of this phenomenon will be presented elsewhere (8).

RIBBON SOLAR CELLS

Solar cells have been fabricated from randomly sampled ribbon blanks, thus ensuring that all qualities of ribbon have been included. Typical junction depths sought were ~ 0.5 μm with phosphorous diffusion being performed in an oxidizing ambient. Cells up to 1 in. $\times$ 4 in. in size have been fabricated (Fig. 16) using Al - Ag contacts formed by evaporation through a mask. The data presented in this paper is from 1 cm $\times$ 2 cm solar cells.

As expected, the particular characteristics of ribbon crystals introduce certain unique problems in solar cell fabrication and performance. The effects of parallel and intersecting boundaries on solar cell properties have been reported elsewhere (7). The effects of non-random properties across the ribbon width discussed in the previous section are also reflected in solar cell performance. By selecting 1 cm $\times$ 2 cm specimens from both the central regions and the edges of 1 in. wide ribbons the influence of the edges on cell performance could be determined. Table III shows a comparative analysis of the properties of cells from the two regions. Significant degradation of cell characteristics from the edges of the ribbon supports the data presented in the previous section.

Spectral response measurements on ribbon solar cells indicated certain unique characteristics in terms of the short wavelength response of the cells. Ribbon cells were typically observed to function better toward the blue end of the spectrum as compared to Czochralski cells made under identical conditions. Figure 17 shows this result. The effects of die purification (vacuum heat treatment and halogen treatment as discussed in the Ribbon Characteristics section) are also

Table III. Solar Cell Data for Specimens Selected from Ribbon Edges and Ribbon Center

Type of Cell	No. of Cells	V_{oc} (mV)	I_{sc}/A (mA/cm^2)	P_{max}/A (mW/cm^2)	Fill Factor	Reverse Leakage (μA)
			Mean Values			
Center	7	529	18.7	7.0	0.71	620
Edge	7	516	17.8	5.8	0.62	2.1 mA

indicated. The reduced response of the ribbon cells in the red end of the spectrum is as expected. (The HCl die purification treatment shows the expected improvement in red response). The blue response however, is observed to be better for ribbon solar cells as compared to Czochralski cells. Typically, blue response can be improved by shallower junction depths (12). Consequently the junction depths for a large number of ribbon and control Czochralski specimens were measured and a difference of ~50% was observed in the depths with the ribbon specimens having shallower junctions when diffused under identical conditions. The mechanism involved in this phenomenon is being investigated and will be reported shortly (13).

Figure 18 shows typical I-V characteristics of current state-of-the-art ribbon solar cells. Typical efficiencies of 6 to 10% under approximate AM0 conditions have been realized, which compare very favorably with conventional Czochralski solar cells.

CONCLUSIONS

One inch wide ribbons ~8 to 10 mils thick have been grown continuously to various lengths up to 65 ft. The carbon dies used show no observable distortion or erosion indicating that continuous ribbon growth can be achieved with carbon dies.

Purification procedures adopted have demonstrated that impurities in the carbon dies can be reduced to improve the purity of the ribbons.

An initial study of defect distributions and structure property relatioships has shown that defect impurity association appears to cause the major problem in ribbon crystals. Improvements in electrical characteristics can be achieved by suitable reductions in both impurity content and defect densities. The use of resistance heated ribbon growth systems with controllable thermal environments has reduced defect densities markedly.

Solar cell efficiencies attainable with appropriate device process technology in ribbon crystals are around 6 to 10% under AM0 illumination conditions. These efficiencies have been attained with a current state-of-the-art material which includes relatively high densities of twins and dislocations in addition to transition metal impurities. Improvements in ribbon characteristics can be achieved by more refined thermal design of growth systems, improved purity, and a reduction in and control of defect densities and distribution.

ACKNOWLEDGEMENTS

APPENDIX

The collection efficiency $Q(\lambda)$ of a photovoltaic cell can be expressed as:

$$Q(\lambda) = \frac{J_{s.c.}(\lambda)}{q\,N_{abs}(\lambda)} \tag{1}$$

where

$J_{s.c.}(\lambda)$ = Short circuit density of the cell, (amp/cm^2)

$N_{abs}(\lambda)$ = Photon flux density being absorbed in the cell, $(photon/cm^2\ sec)$.

= $No\,(1-R)\,(1-e^{-\alpha(\lambda)\ell})$

and

No = Incident photon flux density, $(photon/cm^2\ sec)$.

R = Reflectivity of the cell surface.

$\alpha(\lambda)$ = Absorption coefficient as a function of photon wavelength λ, (cm^{-1}).

ℓ = Thickness of the cell, (cm).

By programming the expression for $Q(\alpha)$ formulated by Dale and Smith [14] in such a form that the input parameters depend on (for an N^+/P junction): the minority carrier diffusion length Ln in the p-type base material, junction depth Xj, surface layer carrier mobility μ_p, and lifetime τ_p, surface impurity concentration to the impurity concentration ratio Ns/NB, cell thickness ℓ, and surface recombination velocity Vs, the value of $Q(\alpha)$ the total collection efficiency can be calculated [15]. The conversion of $Q(\alpha)$ to $Q(\lambda)$ is accomplished by using the absorption data of Dash and Newman [16].

137

REFERENCES

1. B. Chalmers, H. E. LaBelle, Jr., A. I. Mlavsky, J. Crystal Growth, **13/14,** 84 (1972).

2. J. C. Swartz, T. Surek, and B. Chalmers, J. M:·. Sci., **4,** 255 (1975).

3. H. E. Bates, F. H. Cocks, A. I. Mlavsky, IEEE Photovoltaic Specialists Conference Record, 9th, (1972) p. 386.

4. H. E. Bates, D. N. Jewett, and V. E. White, IEEE Photovoltaic Specialists Conference Record, 10th (1973) p. 197.

4a. T. F. Ciszek, Mat. Res. Bull., **7,** 731 (1972).

5. Industrial Graphite Engineering Handbook, Union Carbide Corporation, p. 605 (1970).

6. J. C. T. Ho and K. V. Ravi, to be published.

7. H. B. Serreze, J. C. Swartz, G. Entine and K. V. Ravi, Mat. Res. Bull. **9,** 1421 (1974).

8. A. K. Sood, C. V. Hari Rao, H. E. Bates and K. V. Ravi, Recent News Paper No. 424 Spring Meeting of the Electrochemical Society, Toronto (1975).

9. J. J. Larder, H. Schreiber and T. M. Buck, Appl. Phys. Letters, **3,** 206 (1963).

10. K. V. Ravi, C. J. Varker and C. E. Volk; J. Electrochem. Soc. **120,** 533 (1973).

11. K. V. Ravi and C. J. Varker; Appl. Phys. Letters, **25,** 69 (1974).

12. J. Lindmayer and J. F. Allison, COMSAT Tech. Rev. 3, 1 (1973).

13. H. B. Serreze and K. V. Ravi, to be published.

14. B. Dale and F. P. Smith, J. Appl. Phys., **32,** 1377 (1961).

15. J. C. T. Ho, A. Kirkpatrick and F. T. C. Bartel, NASA Contract No. NAS2-5516, Ames Research Center (1970).

16. W. C. Dash and R. Newman, Phys. Rev. **99,** 1151 (1955).

(a)

SI

Si C

GRAPHITE DIE

(b)
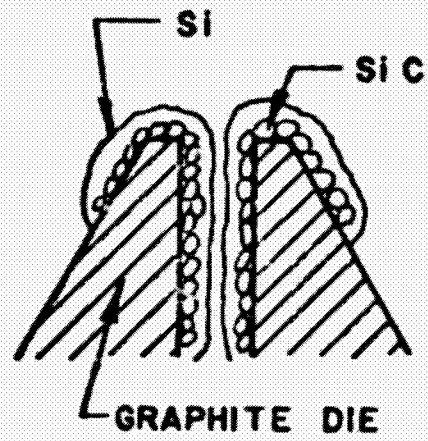
Fig. 1. Typical examples of dies from which short (< 10 ft) and long (> 40 ft)
ribbons have been grown (a and b respectively).

139
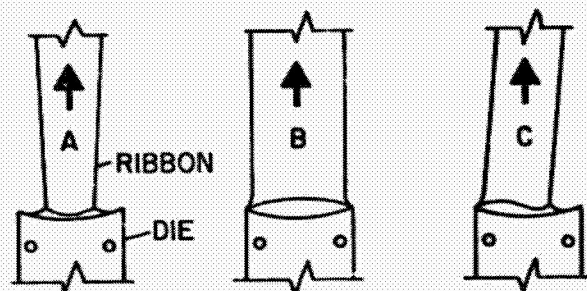
Fig. 2. Schematic sketches of meniscus shapes. See text for discussion.

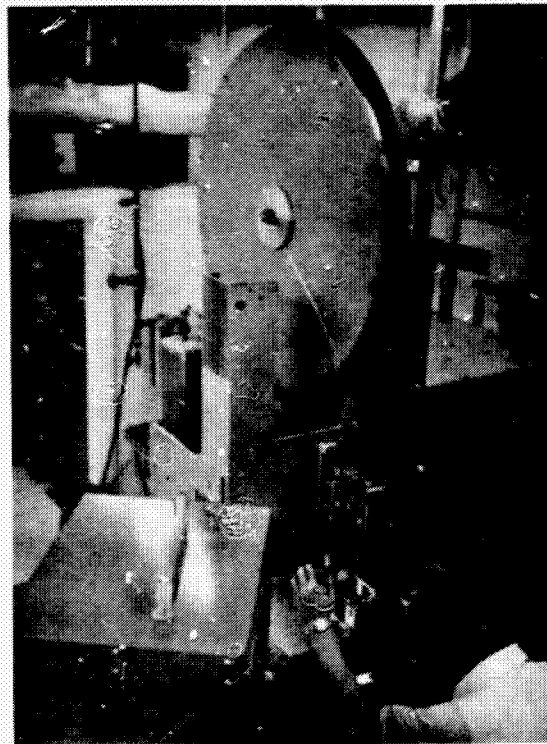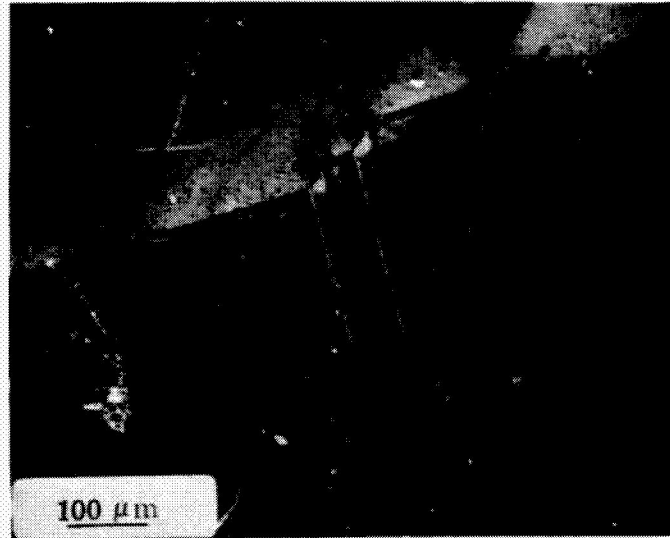Fig. 3. Typical example of an rf heated ribbon growth apparatus.
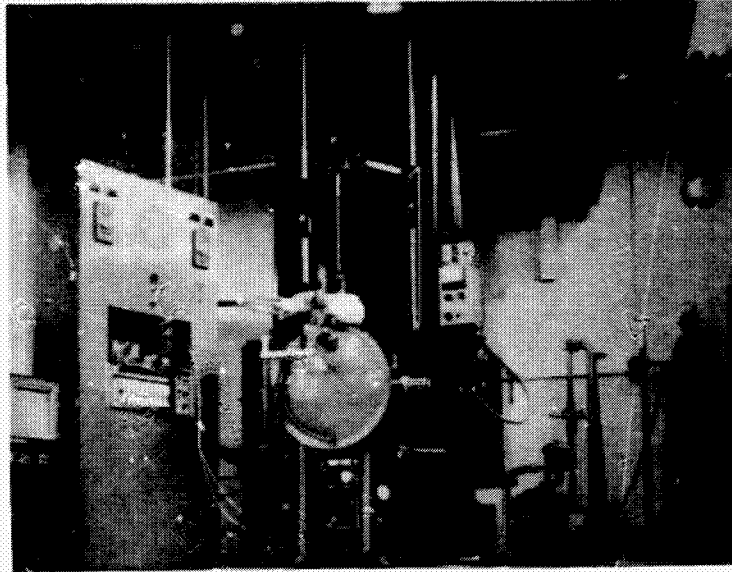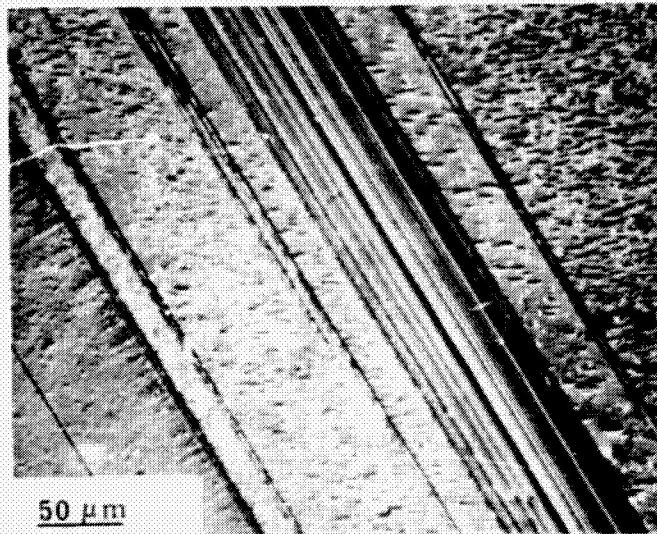
Fig. 4. Resistance heated ribbon growth apparatus.

Fig. 5. Approximately 3 ft diameter reeling mechanism mounted on a continuous belt puller. The ribbon crystal can be observed emerging from the belt puller and on the reel.

141

(a)

100 μm

(b)

50 μm

Fig. 6. Typical examples of growth twins (a) and deformation twins (b). Growth twins are typically wide and generally not associated with dislocation. Deformation twins often occur as closely spaced linear boundaries frequently in association with dislocations.

142
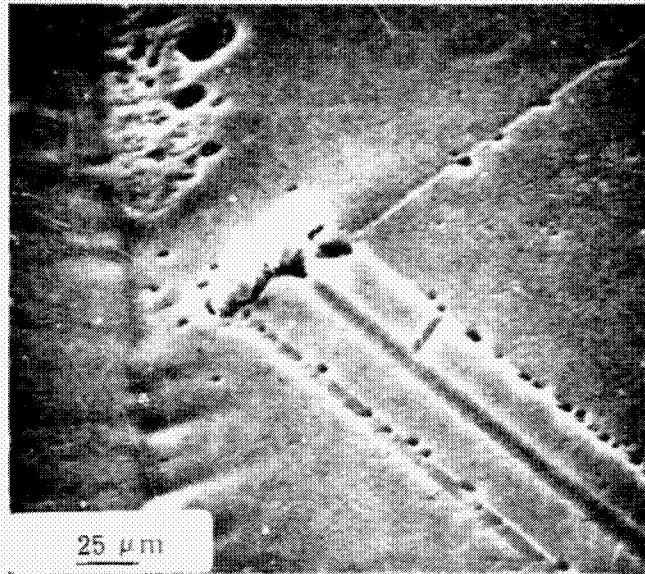
Fig. 7. Twin nucleation from SiC particles embedded in the ribbon.
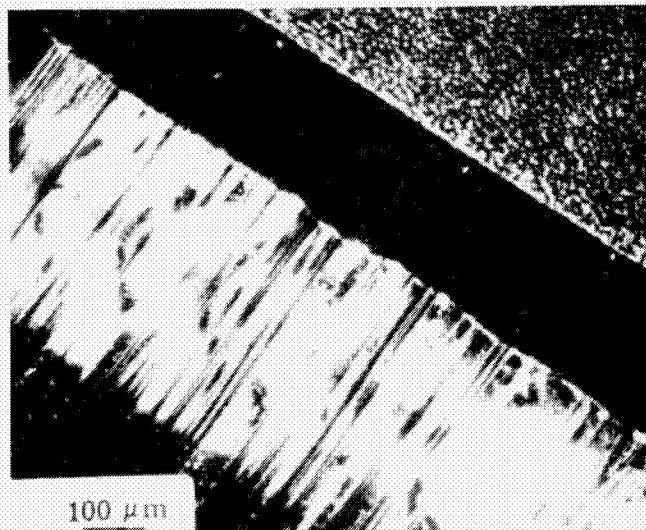
Fig. 8. Twin nucleation at the seed crystal interface.
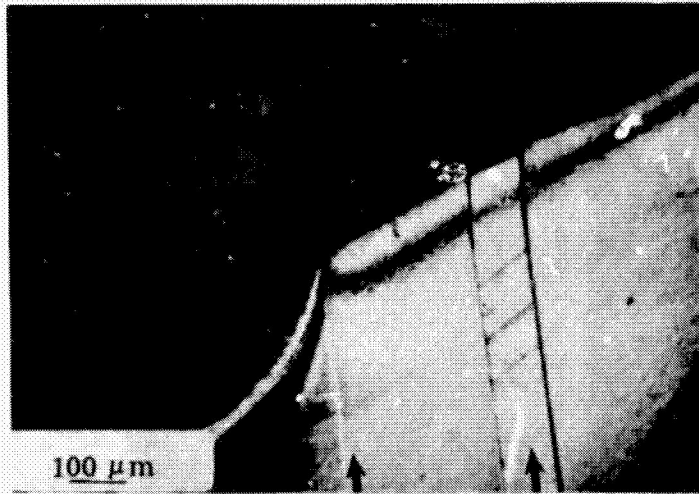
Fig. 9. Twin nucleation due to growth instabilities as represented by changes in ribbon dimensions. Arrows indicate regions of the ribbon which have changed dimension locally and nucleated defects
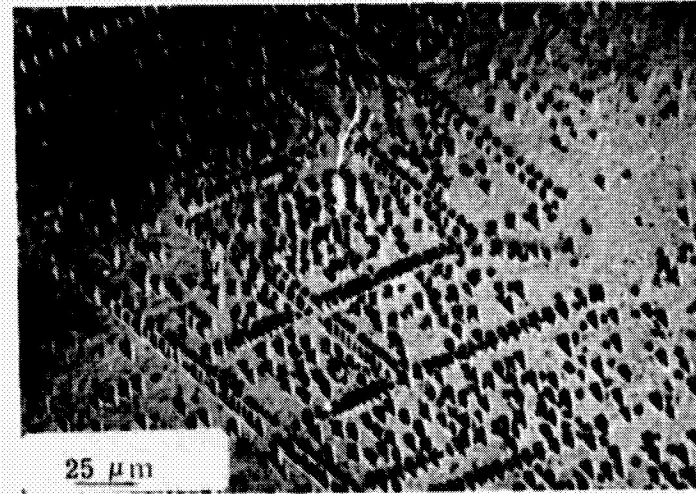
Fig. 10. Deformation induced dislocations aligned along close packed planes. Dislocation pile-ups are also observable in the micrograph.
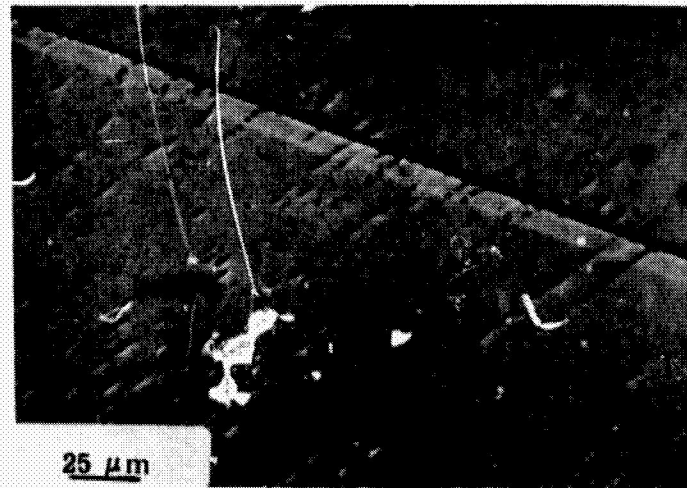
Fig. 11. Dislocation pile-ups against twin boundaries.
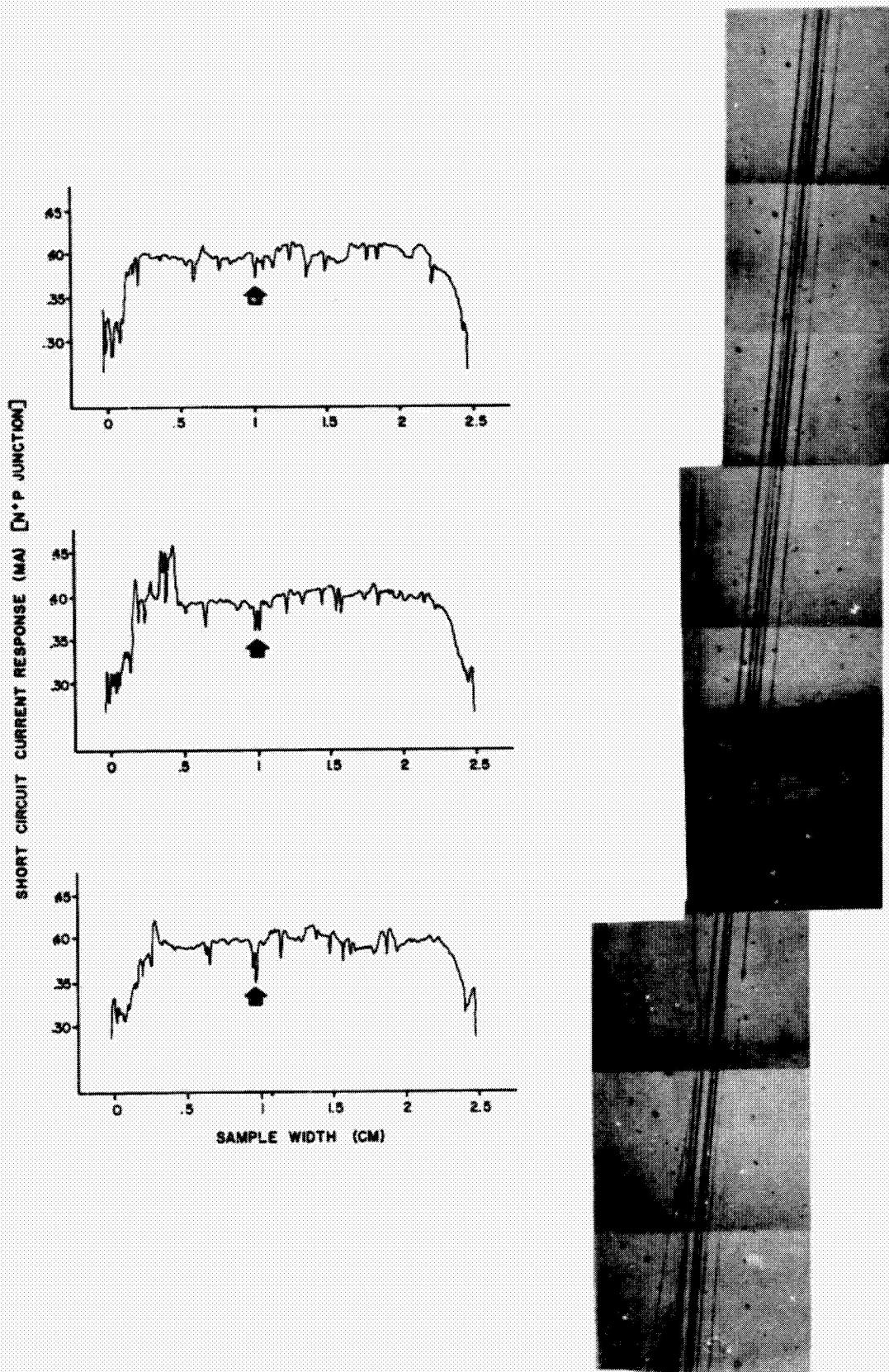
Fig. 12. Short circuit current response plotted as a function of distance across the ribbon width. The three plots were obtained from three regions along the ribbon length. Micrograph shows twin boundaries which caused the particular current indicated by the arrows on the plots.
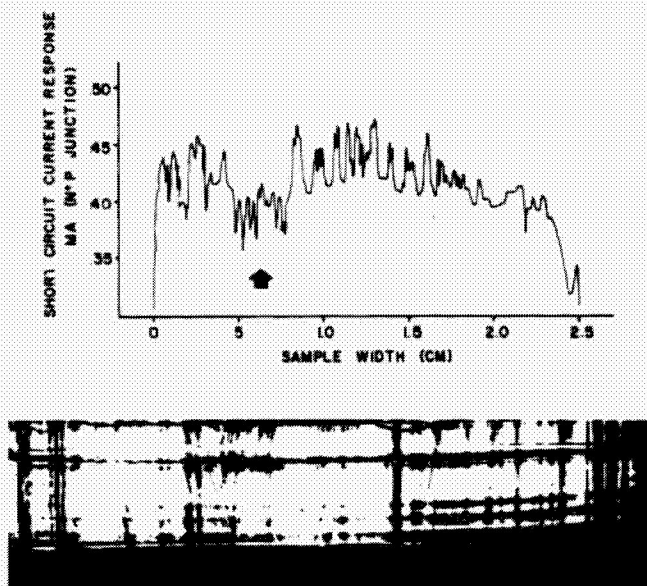
Fig. 13. The effect of intersecting boundaries on laser beam induced short circuit current. Arrow indicates the region on the plot corresponding to the region in the ribbor containing intersecting boundaries.
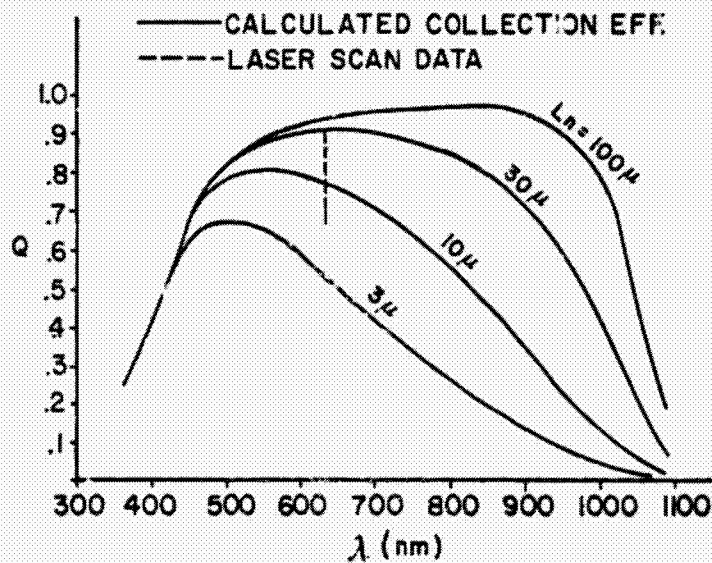

Fig. 14. Theoretically determined spectral response for different values of diffusion lengths in the base region. The laser scan data is superimposed over the theoretical plots. Data used to obtain the plots were: $X_j = 0.25$ μm; $N_S/N_O = 10^5$; $\mu_p = 10$ cm^2/V·sec; $\tau_p = 10^{-10}$ sec; $\ell = 10$ mils; $V_s = 10^5$ cm/sec.
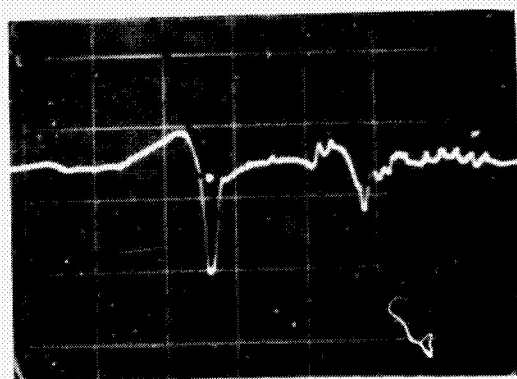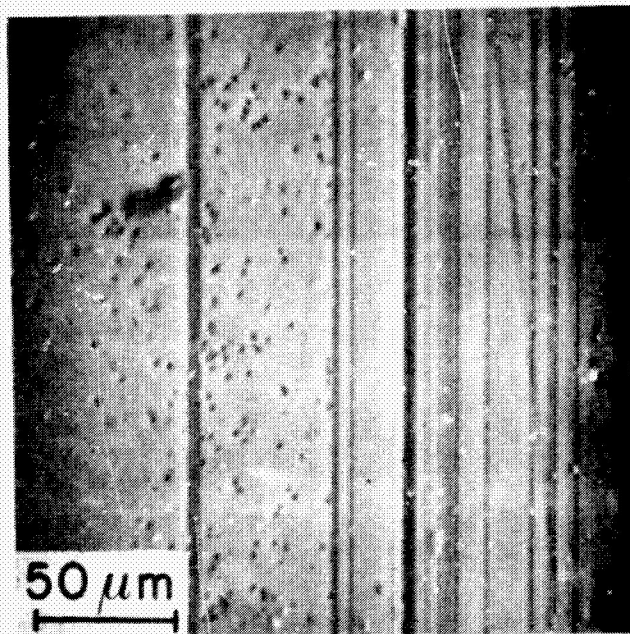
146

Fig. 15. Secondary electron image of linear boundaries in a ribbon crystal. Waveform shows the EBIC signal when the electron beam is scanned across the boundaries. A direct correlation between the boundaries and a local reduction in the EBIC is observed.
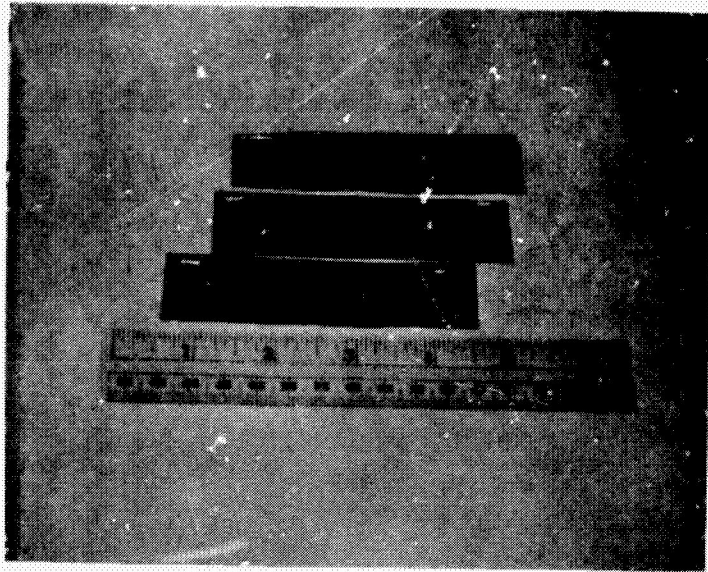
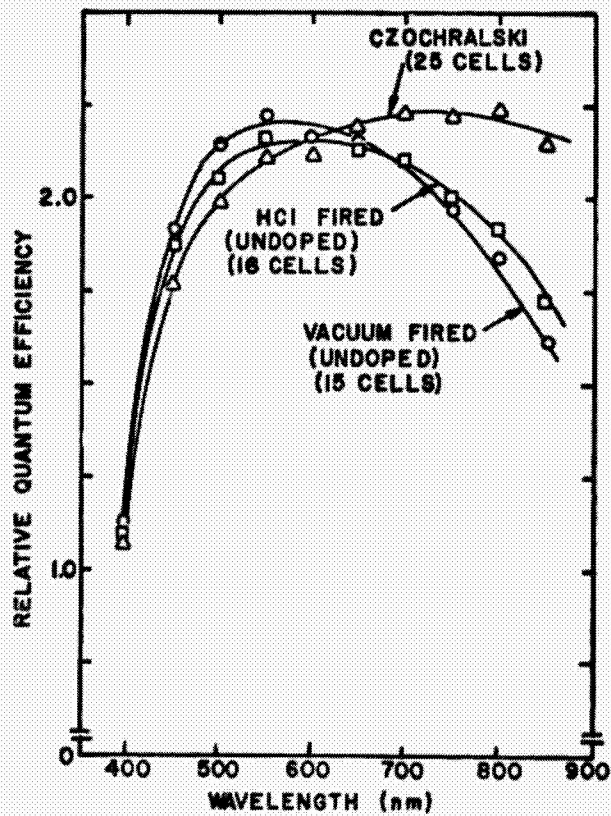Fig. 16. Typical examples of 1 in. × 4 in. ribbon solar cells.

Fig. 17. Comparison of spectral response measurements made on Czochralski and ribbon solar cells. See text for discussion.
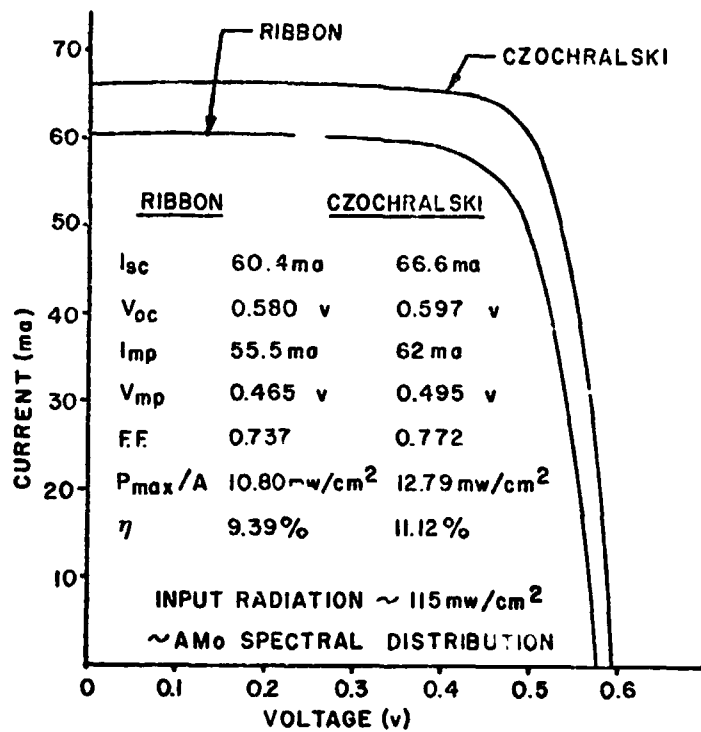
148

Fig. 18. Typical I-V characteristics of current state-of-the-art ribbon solar cells. This data was obtained from ribbons displaying typical defect structures listed in Table I. An I-V curve from a control Czochralski cell is also shown. The cells have been AR coated.

SILICON RIBBON GROWTH USING A
CAPILLARY ACTION SHAPING TECHNIQUE

G. H. Schwuttke/T. F. Ciszek/A. Kran
International Business Machines Corp.
East Fishkill Laboratories
Hopewell Junction, New York   12533

ABSTRACT

A review of work performed since the inception date
(May 8, 1975) is presented, along with an outline of
the project concept and work plan (Figs. 1-3).

The crystal growth method involves Meniscus shaping at
the vertex of a wettable die. As ribbon growth depletes
the melt meniscus, capillary action supplies replacement
material (Fig. 4). Because of the die/melt proximity,
a durable, nonreactive die is desirable. A number of
materials (Fig. 5) have been collected for die evaluation
and are being machined. Crystal growth to date has been
done with graphite and silicon carbide dies. Graphite
dies lead to particle inclusions in the ribbon surface.
We have positively identified the particles as beta silicon
carbide (Fig. 6). Silicon carbide particles and carbon
cause defect nucleation in otherwise defect-free ribbons
(Fig. 7). We have grown a number of 12 mm wide x 0.5 mm
thick x 1 m long ribbons to thoroughly characterize the
state-of-the-art multi-crystalline ribbons, and are in the
process of scale-up to 25 mm widths while studying process
changes for improved ribbon structure.

Two projects which were begun before the inception date were completed during the past two months. An expression for maximum potential ribbon growth rates was derived an the results are shown graphically in Figs. 8-9. Current rates for 0.05 cm thick ribbons (about 2 cm/min.) are approximately 30% of the maximum value. The second completed project involved the growth of silicon tubes 6 mm in wall thickness, and over 1 m in length by the capillary action shaping technique (Fig. 10-12). Tube structure was similar to that of ribbons. Planar defects and some large angle grain boundaries were present, with the largest grains extending over one quarter of th tube circumference.

In conjunction with and support of the technology development effort, an economic evaluation and compute -aided simulation of materials processes and resources is being performed for the purpose of clarifying the complex interactions between economic and physical variables. Objectives are listed in Fig. 13.

To date, a methodology for analyzing a given processing step has been defined and ribbon pulling was chosen as the initial modeling effort. The assigned parameters of the mathematical model are shown in Figure 14, and Figure 15 lists the parameters which are subsequently calculated. The data flow model is shown in Figure 16. An example of the computer generated input/output formats is presented in Figures 17 and 18. Figures 19 through 23 address the remaining review items.

SILICON RIBBON GROWTH USING A CAPILLARY
ACTION SHAPING TECHNIQUE

G. H. SCHWUTTKE, PROGRAM MANAGER

914-897-3140

JPL CONTRACT NUMBER: 954144

(SUBCONTRACT UNDER NASA CONTRACT NAS7-100)
(TASK ORDER NO. RD-152)
EFFECTIVE DATE OF CONTRACT: 5/8/75
CONTRACT EXPIRATION DATE: 12/31/76
CONTRACT AMOUNT: $214,133.

OBJECTIVES

1. TECHNOLOGICAL ASSESSMENT OF RIBBON GROWTH OF
   SILICON USING A CAPILLARY ACTION SHAPING TECHNIQUE.

2. ECONOMIC EVALUATION OF RIBBON SILICON GROWN BY A
   CAPILLARY ACTION SHAPING TECHNIQUE AS LOW COST
   SILICON.

SYNOPSIS OF PROGRAM OF STUDY, PRINCIPAL INVESTIGATORS

1. CRYSTAL GROWTH OF SILICON RIBBONS (T. F. CISZEK)

2. CHARACTERIZATION OF SILICON RIBBONS (G. H. SCHWUTTKE)

3. ECONOMIC EVALUATIONS AND COMPUTER AIDED SIMULATION
   OF RIBBON GROWTH (A. KRAN)

STATEMENT OF WORK

1. EVALUATION OF DIE MATERIALS AND DESIGNS

2. DETERMINATION AND OPTIMIZATION OF BASIC
   GROWTH PROCESSES

3. STUDY PROCESS EFFECTS ON RIBBON PROPERTIES

4. STUDY REQUIREMENTS FOR MULTIPLE AND
   CONTINUOUS GROWTH

5. EVALUATION OF CHARACTERIZATION PROCESSES

6. ECONOMIC ANALYSIS OF RIBBON AND CZOCHRALSKI
   TECHNIQUES

3

2

1

Ribbon

Capillary
Die

Melt

Crucible
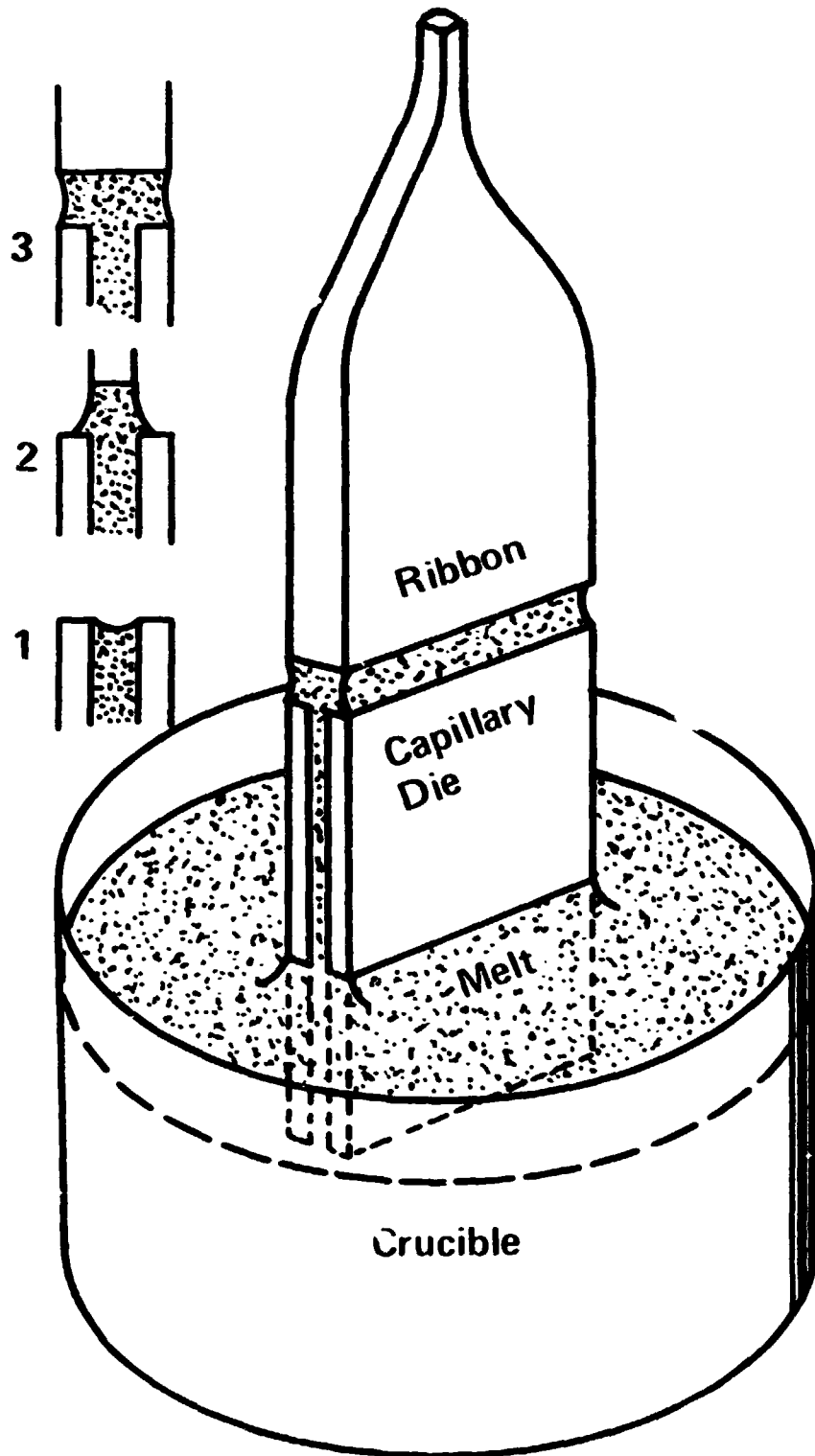
DIE MATERIALS UNDER INVESTIGATION

ZIRCONIUM BORIDE (HOT PRESSED

TITANIUM BORIDE (HOT PRESSED)

BORON CARBIDE (HOT PRESSED)

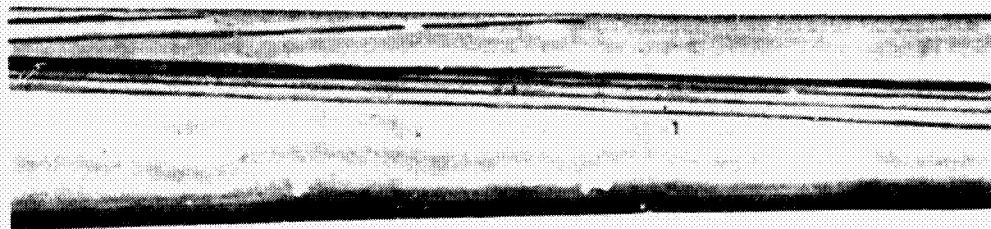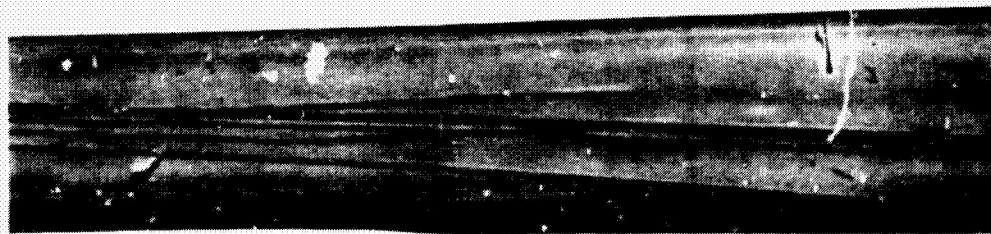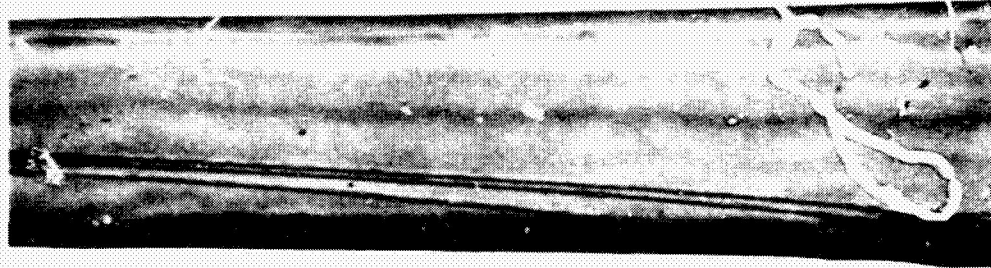ALUMINUM BORIDE

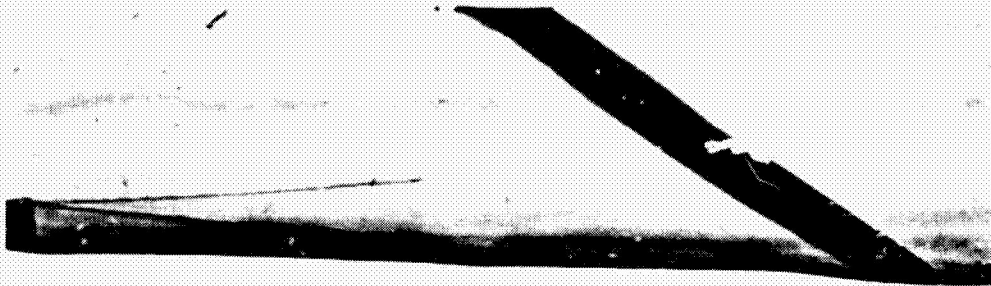SILICON NITRIDE

SILICON CARBIDE (RECRYSTALLIZED)
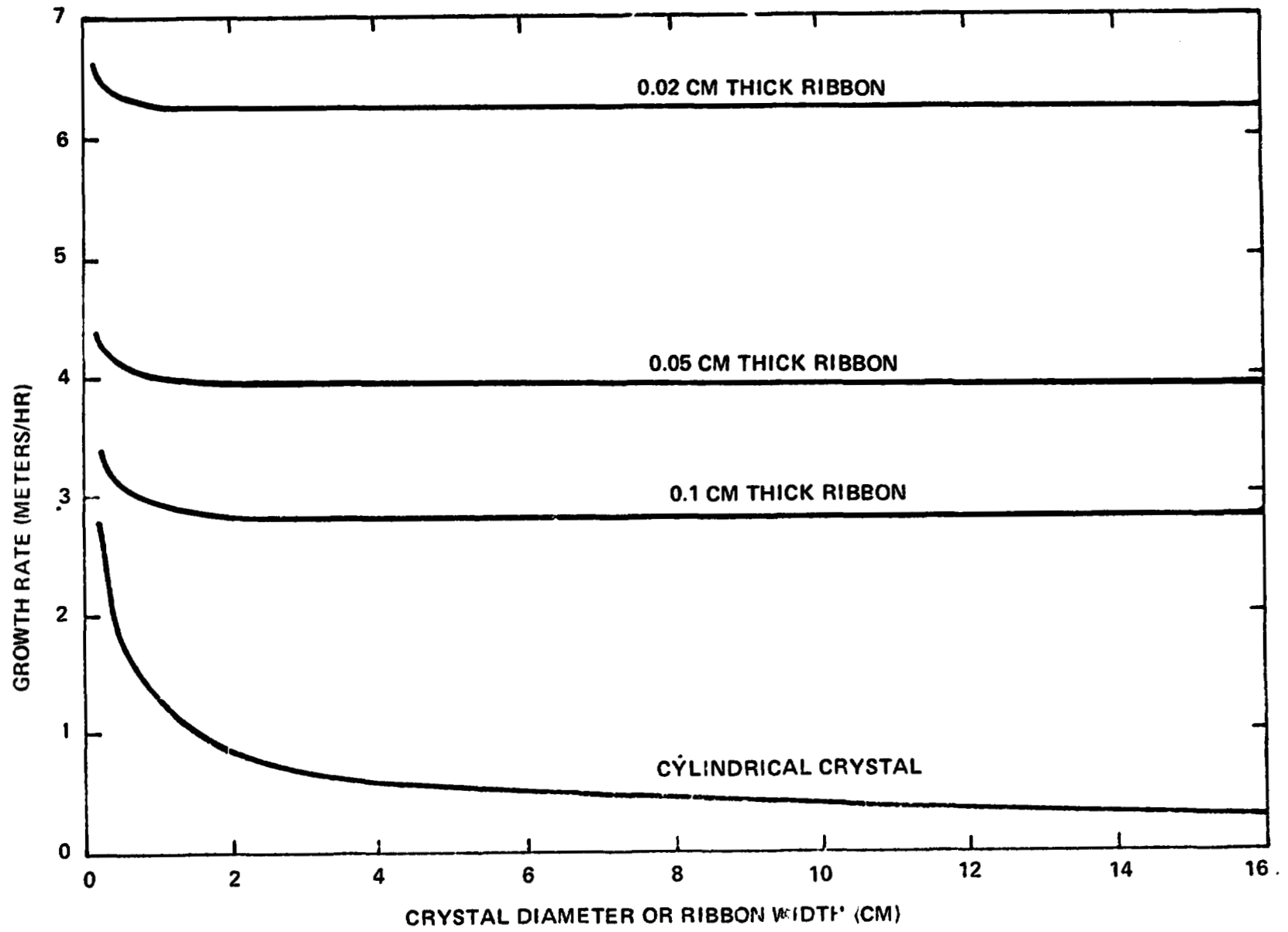
VITRIOUS CARBON

IDENTIFICATION OF YELLOWISH-GREEN INCLUSION

CRYSTAL			ASTM CARD #1-1119 Beta SiC	
d	I_O		d	I/I_1
2.51	S		2.51	100
2. ᴖ	M		2.17	20
1 ᴖ4	M		1.54	63
1.315	M		1.31	50
1.27	W		1.26	5
			1.09	6
1.00	W		1.00	18
0.975	W		0.97	6
0.89	W		0.89	13
0.84	W		0.84	10

TUBE

DIE

MELT

CRUCIBLE
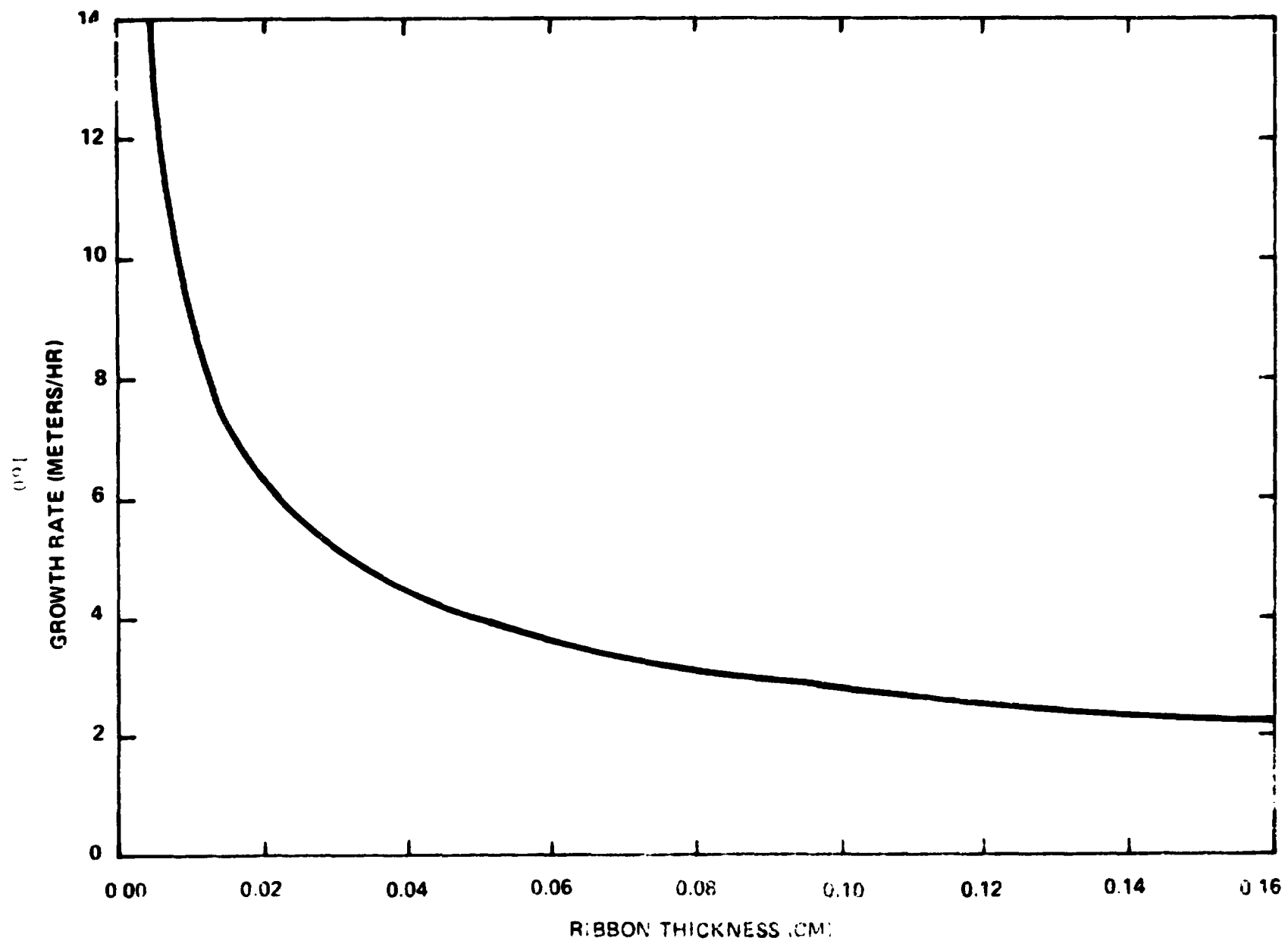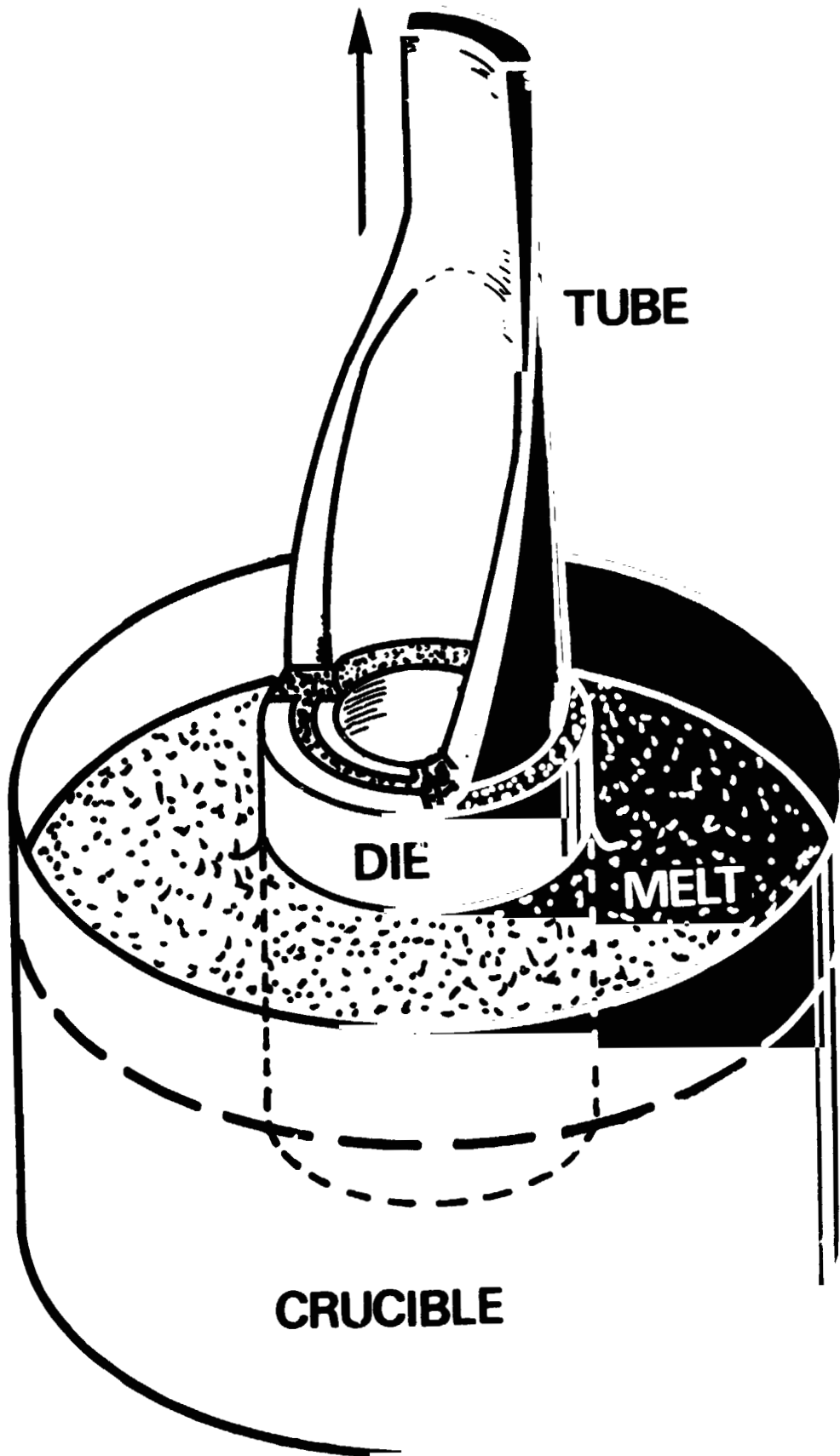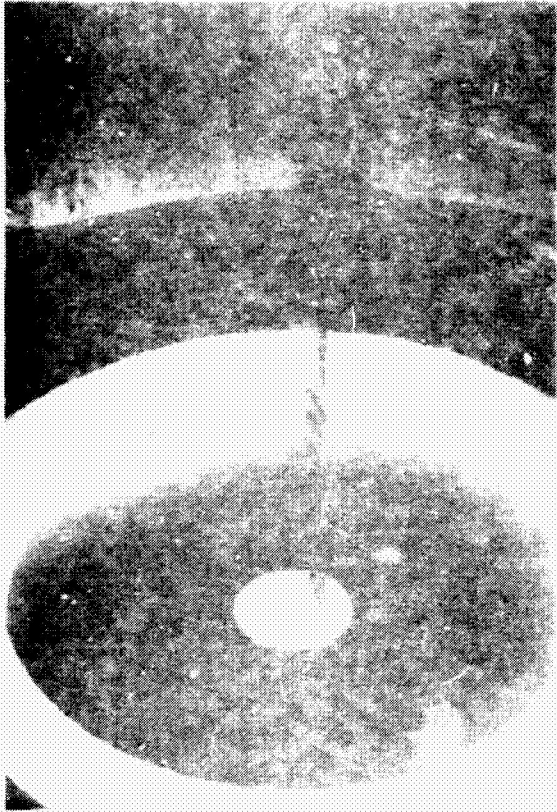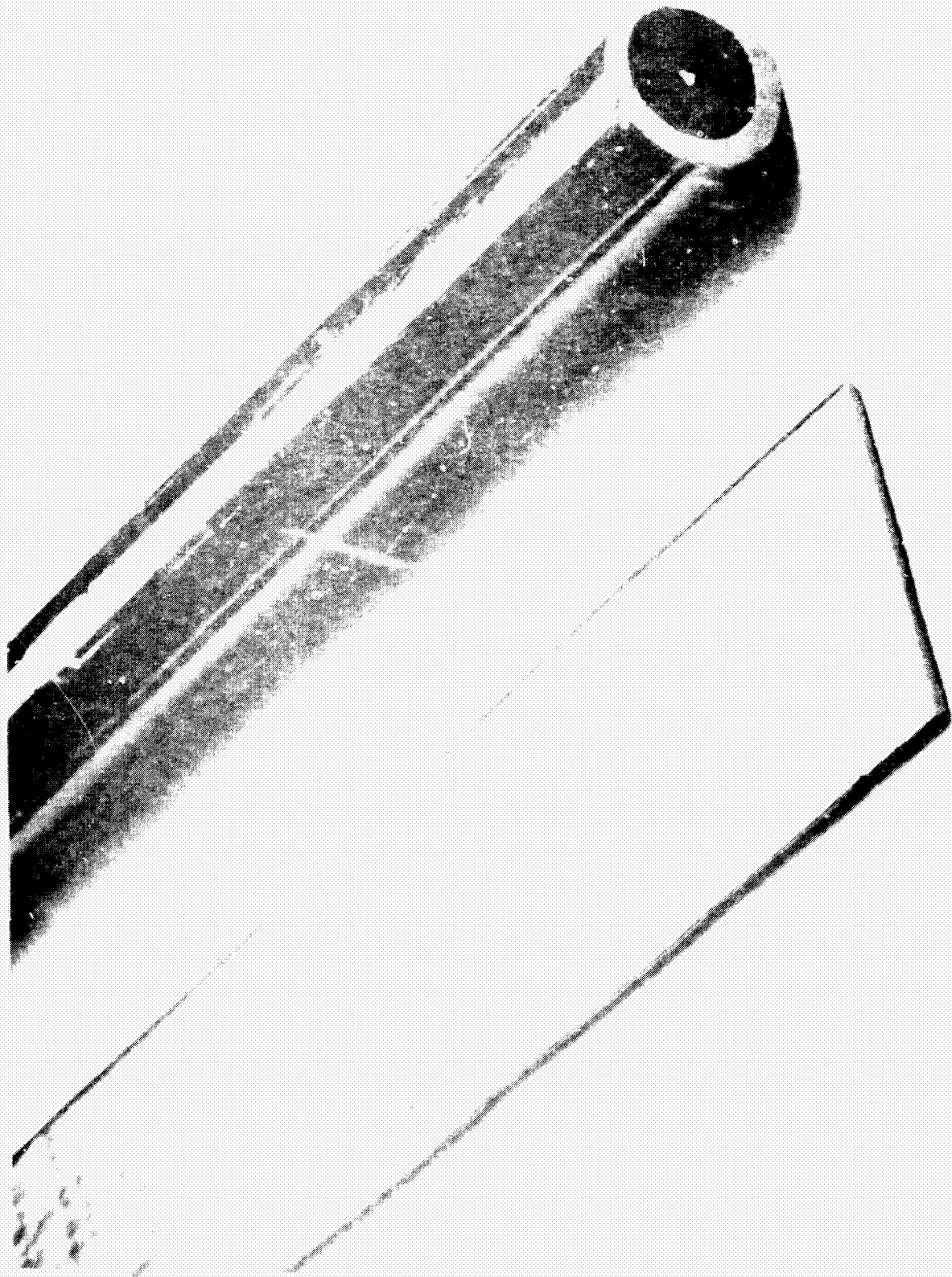
OBJECTIVE OF COMPUTER AIDED MODELING

o TO UNDERSTAND THE RESPECTIVE IMPORTANCE OF
   PARAMETERS AND THEIR ASSIGNED VALUES

o TO AID IN SENSITIVITY STUDIES

o TO ASSESS THE IMPACT OF TECHNOLOGY IMPROVEMENTS
   ON THE ECONOMIC OUTLOOK FOR PHOTOVOLTAICS

o TO GAIN INSIGHT ON ASSUMPTIONS AND TECHNOLOGY
   PROJECTIONS

MATHEMATICAL MODEL

1. ASSIGNED PARAMETERS

CC = CRUCIBLE COST, $

CH = ENERGY TO OPERATE EQUIPMENT, KW

CP = POWER COST, $/KWH

DS = SILICON DENSITY, 2.33 G/CM^3

EC = CONVERSION EFFICIENCY, %

ED = ENERGY DENSITY, PEAK AT AM1, %

EP = EQUIPMENT PRICE, $

HW = WORK WEEK, HOURS

FC = FACTOR, %

IN = INTERST, %

LP = POLY SILICON COST, $/KG

LR = REMELTED MATERIAL, %

LY = POLY YIELD TO RIBBON, %

MA = MACHINE AVAILABILITY, %

NU = NUMBER OF YEARS

PE = ANNUAL SALARY OF ENGINEER, $

PS = ANNUAL SALARY OF SUPERVISOR, $

PT = ANNUAL SALARY OF TECHNICIAN, $

RG = RIBBON GROWTH RATE, M/HR

RS = RIBBONS GROWN SIMULTANEOUSLY

RT = RIBBON THICKNESS, MM

RW = RIBBON WIDTH, CM

RY = RIBBON GROWTH YIELD, %

2. CALCULATED PARAMETERS

$\underline{A}G$ = AREA GROWTH RATE, M^2/HR

$\underline{C}R$ = CAPITAL RECOVERY FACTOR

$\underline{D}C$ = DIRECT COST, $\$/M^2$

$\underline{E}C$ = CAPITAL EQUIPMENT COST, $\$/M^2$

$\underline{G}A$ = GENERAL & ADMINISTRATIVE COST, $\$/M^2$

$\underline{L}C$ = POLY SILICON CO⌐ $\$/M^2$

$\underline{N}C$ = ENERGY COST AT MATERIAL LEVEL, $\$/KW$

$\underline{N}H$ = WORKING HOURS PER YEAR

$\underline{P}C$ = PERSONAL COST, $\$/M^2$

$\underline{P}R$ = PROFIT, $\$/M^2$

$\underline{O}H$ = OVERHEAD, $\$/M^2$

$\underline{S}S$ = SERVICES & SUPPLIES, $\$/M^2$

$\underline{T}O$ = COST OF TOTAL OPERATIONS, $\$/M^2$

$\underline{Y}F$ = YIELD FACTOR

DATA FLOW MODEL
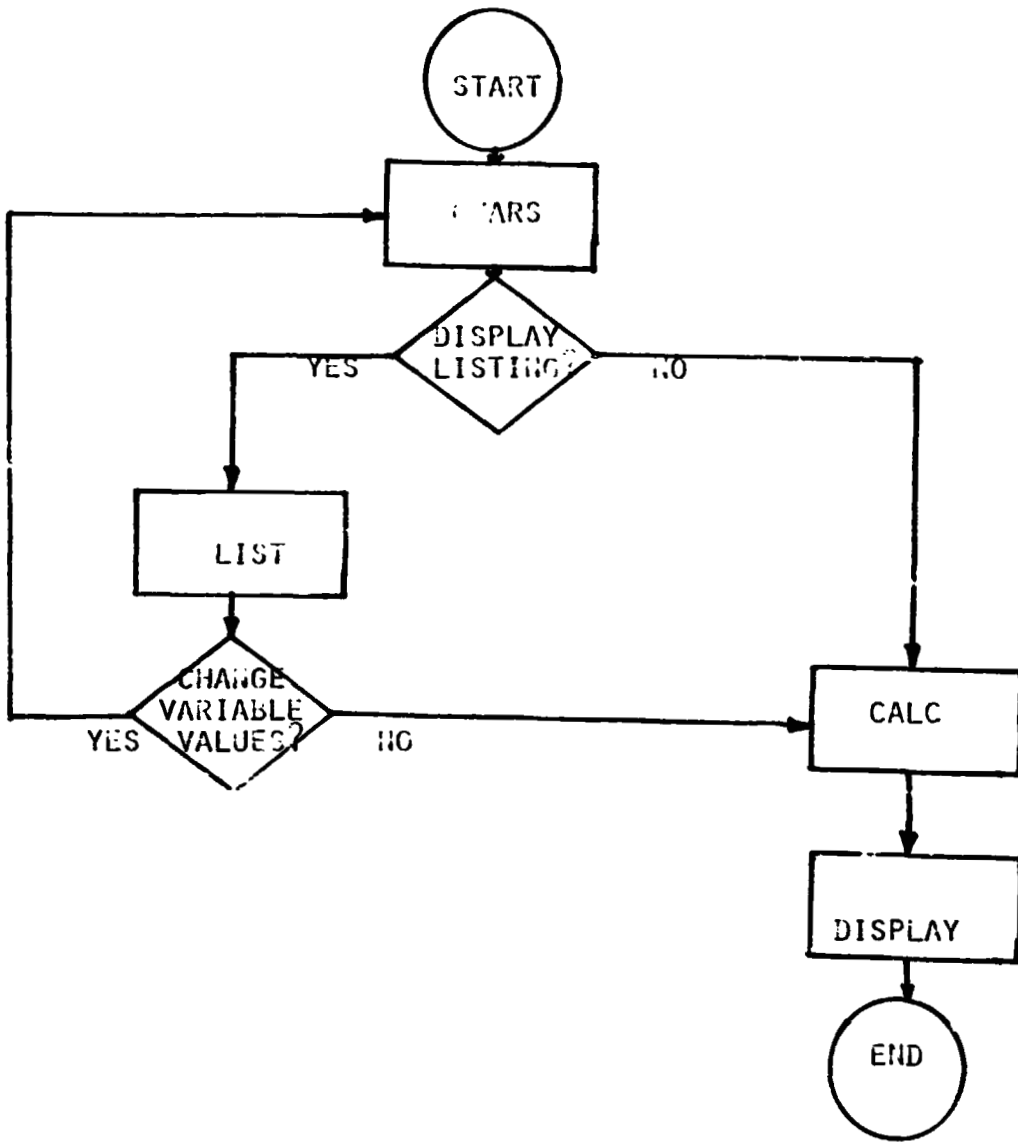
LIST OF RIBBON PARAMETERS AND THEIR ASSIGNED VALUES

RIBBON DATA
1   RIBBON GROWN SIMULTANEOUSLY - 1 1 1
2   RIBBON WIDTH, CM - 3 3 3
3   RIBBON GROWTH RATE,M/HR - 2.3 2.3 2.3
4   RIBBON THICKNESS, MM - 0.2 0.2 0.2
5   YIELD OF GOOD RIBBON, PERCENT - 60 70 80

    DIRECT COST
6   RIBBON FURNACE, DOLLARS - 25000 25000 25000
7   EQUIPMENT LIFE, YEARS - 7
8   INTEREST RATE, PERCENT - 8
9   EQUIPMENT AVAILABILITY, PERCENT - 70

10 PERSONNEL PER SHIFT
11   NO. OF SUPERVISORS - 0.05 AT A YEARLY RATE OF - 25000
12   NO. OF ENGINEERS - 0.1 AT A YEARLY RATE OF - 20000
13   NO. OF TECHNICIANS - 0.5 AT A YEARLY RATE OF - 10000

14 POLY SILICON COST, DOLS/KG - 65 65 65
15 POLY YIELD TO RIBBON,PERCENT - 80 80 80

16 SERVICES AND SUPPLIES
17   ONE CRUCIBLE PER DAY AT A COST OF - 30 DOLLARS
18   POWER COST AT - 0.05 DOLLARS PER KWH
19   ENERGY TO OPERATE EQUIPMENT - 20 KW

    OVERHEAD - 50 PCT OF PERSONNEL+ 10 PCT OF RAW MATL COST
    G AND A - 10 PERCENT OF DIRECT COST+OVERHEAD

    PROFIT BEFORE TAX, PERCENT - 10 OF DC+O/H+G&A

    MISCELLANEOUS
20 WORKWEEK, HOURS - 120
21 CONVERSION EFFICIENCY, PERCENT -   7.5
22 ENERGY DENSITY AT AM1,KW/M SQ PEAK - 1

ECONOMICS OF SILICON RIBBON - ONE RIBBON PULLER

PRINTED FROM A. KRAN'S SF WSS: 06.33 HOURS, 07/14/73

RIBBONS GROWN SIMULTANEOUSLY	1.00	1.00	1.00
RIBBON WIDTH, CM	3.00	3.00	3.00
AVG AREA GROWTH RATE, SQ M/HOUR	0.33	0.33	1.04
COMBINED YIELD FACTOR	0.48	0.50	0.64
DIRECT COST IN DOLS/SQ METER			
EQUIPMENT CAPITAL RECOVERY	27.02	25.67	20.71
PERSONNEL	142.34	122.01	100.75
POLY SILICON COST	63.10	54.00	47.33
SERVICES/SUPPLIES	67.29	57.00	50.47
SUBTOTAL:	300.33	257.44	225.26
OVERHEAD COST IN DOLS/SQ METER	74.20	64.33	56.41
GGA EXPENSES IN DOLS/SQ METER	37.45	32.15	28.17
PROFIT IN DOLLARS/SQ METER	41.20	35.58	30.03
TOTAL COST IN DOLS/SQ METER	453.20	388.00	340.02
DOLLARS PER KW	6042.07	5166.42	4544.22

3. PLANNED ACTIVITY TO DATE (3 MONTHS)

DESIGN A COMPUTER-AIDED MODEL TO ESTABLISH

A RELATIONSHIP BETWEEN THE COMPLEX INTERACTIONS

OF ECONOMIC AND PHYSICAL VARIABLES.

PLANNED ACTIVITY FOR NEXT 6 MONTHS

MAJOR PROBLEMS

- USE MODEL TO PERFORM ENGINEERING/ECONOMIC ANALYSIS

NONE

- DEFINE SIMILAR MODEL FOR CHRALSKI GROWTH

- PERFORM COMPARISON STUDIES

SUMMARY OF KEY RESULTS

PLANNED RENEWAL REQUESTS

RIBBON GROWTH MODEL ' "" N DEFINED

AND DEBUGGED. LITTLE   :' " DATE.

TOO EARLY TO FORMULATE PLANS.